Measurements of Total Aerosol Deposition and Validation of Airway Resistance Models in Anatomically Realistic Intrathoracic Conducting Airway Replicas of Children

by

Azadeh Akhavan Taheri Borojeni

A thesis submitted in partial fulfillment of the requirements for the degree of

Doctor of Philosophy

Department of Mechanical Engineering

University of Alberta

ABSTRACT

One objective of this research was to obtain a correlation that quantitatively predicts micrometer-sized aerosol particle deposition in the upper conducting airways (trachea to generation 3) of children. Experiments were conducted using steady inhalation air flow rates to measure the deposition of monodisperse particles with diameters of 3.5–5.5 micro-meter in replicas of the upper tracheobronchial airways of 11 children aged 2–8 years. The total deposition of particles was measured in each replica using gravimetry. Validation was performed by measuring deposition in five adult replicas and comparing with existing published data. Although there is considerable intersubject variability in our data, the empirical correlation of Chan & Lippmann (1980) was found to predict total deposition reasonably well in all of our adult and child replicas.

A second goal of this study was to design an idealized pediatric central conducting airway model that mimics average total particle deposition in the airways of 4-8 year old children. Dimensions of the idealized model were selected based on analytical prediction of deposition in scaled versions of existing adult airway geometries. Validation experiments were then conducted using steady inhalation air flow rate to measure the deposition of monodisperse particles with mass median diameters (MMD) of 3.5, 4.5, 5 and 5.2 micro-meter in the idealized pediatric model. The total deposition of particles was measured using gravimetry. Experimental data confirmed that aerosol deposition in the idealized pediatric central conducting airway geometry was consistent with the average deposition previously measured in 10 realistic airway replicas for children 4-8 years old.

Finally, this thesis describes *in vitro* measurements of the total pressure loss at varying flow rate through anatomically realistic conducting airway replicas of ten children, 4 to 8 years old, and five adults. Experimental results were compared with analytical predictions made using

published airway resistance models. For the adult replicas, the model proposed by van Ertbruggen et al. (*J. Appl. Physiol.* 98:970-980,2005) most accurately predicted central conducting airway resistance for inspiratory flow rates ranging from 15 to 90 L/min. Models proposed by Pedley et al. (*J. Respir. Physiol.* 9:371-386,1970) and by Katz et al. (*J. Biomechanics* 44:1137-1143,2011) also provided reasonable estimates, but with a tendency to over predict measured pressure loss for both models. For child replicas, the Pedley and Katz models both provided good estimation of measured pressure loss at flow rates representative of resting tidal breathing, but under predicted measured values at high inspiratory flow rate (60 L/min). The van Ertbruggen model, developed based on flow simulations performed in an adult airway model, tended to under predict measured pressure loss through the child replicas across the range of flow rates studied (2 to 60 L/min). These results are intended to provide guidance for selection of analytical pressure loss models for use in predicting airway resistance and ventilation distribution in adults and children.

DEDICATION

I would like to dedicate this thesis to Dr. Alireza Vali for his endless support.

ACKNOWLEDGMENT

First of all, I would like to express my gratitude to my supervisors Prof. Warren H. Finlay and Dr. Andrew R. Martin whose guidance and support enabled me to carry out this thesis within the Aerosol Research Laboratory of Alberta (ARLA) at the University of Alberta. It is my pleasure to thank Prof. Michelle L. Noga from the department of radiology and diagnostic imaging for providing CT scans and helping with ethics approval procedures. Thanks also to Greg Wandzilak from PRT/CT center, University of Alberta, Stollery Children's Hospital for his assistance in providing CT images.

I wish to thank Dr. Reinhard Vehring and his research group for sharing the Aerodynamic Particle Sizer.

Furthermore, I am grateful to Andrew Campbell, Ryan Shoults, Dave Waege and Roger Marchand for their technical support and help throughout this project.

Andrew Grosvenor and Jamie Schmitt from the Institute for Reconstructive Sciences in Medicine (iRSM) are acknowledged for their technical help in fabricating the replicas.

Ms. Helena Orszanska is gratefully acknowledged for her help on the UV spectroscopy chemical asseys.

I would like to thank my family and friends in Iran, The Netherlands and Canada for all their companionship, understanding and support in stressful times.

During my stay in Edmonton I spend much time with my dear friends Fatemeh Miri and her respected husband, Alireza Vali, Sama Naderi and her family, Samar and Iman Shams, Mahshid and Danoush Yousefi, Pirooz Taef, Mahin and Sohrab Bahrami, Mehrdad and Lida Kiai. I wish to thank them for all their support.

Lastly, I would like to express my sincere gratitude to Dr. Soheil Homayouni for all his interest, encouragement, help and continuous support throughout the years.

Azadeh Akhavan Taheri Borojeni
October, 2014
Edmonton, AB, Canada

Table of Contents

List of Tables

List of Figures

CHAPTER 1 : SUMMARY AND INTRODUCTION

1.1 Background

The first step in evaluating risks associated with exposure to airborne particles and also in investigating the efficiency of pharmaceutical drug delivery devices is to predict the amount of aerosol deposition in the human respiratory tract (Kelly et al. (2004)). Aerosol deposition has been measured extensively by several investigators for different age groups ranging from infant to adult subjects. Traditionally, *in vivo* studies measured total and regional deposition (Stahlhofen et al. (1980); Lippmann (1977); Lippmann et al. (1971); Heyder et al. (1973, 1975); Emmett et al. (1982)).

While *in vivo* experimental studies using radiolabeled tracer particles and gamma scintigraphy technique have determined total and regional particle deposition (Stahlhofen et al. (1981, 1983, 1984); Devadason et al. (1997, 2003); Bowes and Swift (1989); Svartengren et al. (1994); Lippmann and Albert (1969); Lippmann et al. (1971); Newman et al. (1988); Emmett et al. (1982); Itoh et al. (1980); Chua et al. (1994)), radiation exposure and ethical considerations of investigation of radiolabelled deposition (Everard (1994)) have resulted in limited information regarding particle deposition in the respiratory tract of infants and children. Furthermore, *in vivo* studies and experimental observation of particle deposition in human beings are expensive and more difficult to control.

Because of these difficulties in conducting *in vivo* methods, researchers have recently focused on doing experiments using 3D anatomically based human airway replicas. In recent years, modern imaging technics such as magnetic resonance imaging (MRI), computed tomography (CT), and high resolution computed tomography (HRCT) can be used in supplying data for fabricating accurate and realistic airway models. The medical imaging process and generating the computer mesh geometry of the human airways have been considered elsewhere (McRobbie et al. (2003); Ma and Lutchen (2006, 2009)). Most of the *in vitro* studies have focused on extrathoracic airways (Swift (1991); Storey-Bishoff et al. (2008); Golshahi et al. (2011, 2012)) but very few studies have reported

determination of total deposition in the upper tracheobronchial airways of children (Oldham et al. (1997)).

The tracheobronchial region is the proximal part of the intrathoracic airways of the respiratory tract (Cheng et al. (1995)). Several studies investigate total and regional particle deposition in the head airway or extrathoracic region, consisting of nasal and oral cavity, pharynx and larynx (Grgic et al. (2004); Storey-Bishoff et al. (2008); Golshahi et al. (2011, 2012)). However, a limited number of studies have been performed to measure deposition in the intrathoracic region.

The World Health Organization's (WHO) cancer agency announced that 223,000 lung cancer deaths happened because of inhaling toxic air pollutants in 1991 (Szabo et al. (1993)). Histological studies frequently find the intrathoracic conducting airways are a site where lung cancers and other chronic diseases occur (Swift et al. (1992); Cheng et al. (1995); Schlesinger et al. (1972) and Schlesinger et al. (1978)). Therefore, measuring particle deposition and developing deposition models and correlations in tracheobronchial airways is valuable. A better understanding of inhaled particle deposition may also lead to more increased efficacy of aerosol drug devices such as inhalers and nebulizers. Development of more efficient aerosol delivery devices is useful to help to achieve the final goal of improved aerosol therapy and optimal drug delivery. Thus, both from a drug delivery view point and risk assessment analysis of the human respiratory tract, studying particle deposition focusing on the intrathoracic zone (tracheobronchial and alveolar regions) is desirable.

1.2 Lung airway configurations

Over the past decade several lung airway geometries have been proposed. Probably the most recognized model is Weibel's model A (Weibel (1963)). This is a symmetrical simple model which assumes each lung generation bifurcates symmetrically in two identical branches. It is still used in computational fluid dynamics (CFD) simulations (Lambert et al. (2011)) and laboratory studies (Martin and Jacobi (1972); Oldham et al. (1997); Briant and Cohen (1989); Zhang and Kleinstreuer (2001)).

However, considerable intersubject variability and anatomic differences exist. These yield effects on particle deposition in human airway that have not been well characterized, despite it being recognized that there are some main features in the human airway geometry that have a critical effect on the airflow distribution and particle deposition (Harrington et al. (2006)). Such factors should be considered when developing an idealized lung airway geometry (Kleinstreuer and Zhang (2009); Stapleton et al. (2000)). Moreover, semi-empirical correlations and analytical models based on idealized lung geometries are widely employed to predict particle deposition in the human respiratory tract (ICRP (1994); NCRP (1997); Hofmann et al. (1989) and Rudolf et al. (1988, 1990, 1994)).

Current inhalation devices have limited efficiency in reaching the targeted region of the respiratory tract (Kleinstreuer et al. (2008)). This can be combated by increasing the dosage of administration, but this will increase the potential for side effects (Kleinstreuer et al. (2008)). However, this raises a need to employ an idealized geometry which can be used prior to clinical trials to predict the delivery of pharmaceutical particles throughout the conducting airways. It has been argued that employing a single idealized geometry is a good alternative to anatomically accurate replicas (Byron et al. (2010); Finlay et al.(2010)). Recently, in predicting aerosol deposition in the human respiratory tract using *in vitro* testing, adult airway models were scaled to represent a pediatric airway geometry (Below at al. (2013); Bickmann et al. (2008); Delvadia et al. (2012); Golshahi and Finlay (2012); Oldham et al. (1997); Wachtel et al. (2010)). A few numerical studies have been done to investigate particle deposition in idealized hollow upper bronchial airway replicas (Kleinstreuer and Zhang (2003)). These airway models were based on Weibel's lung geometry (Weibel (1963)) and they were symmetrical. However, a limited attempt has been performed regarding the generation of idealized asymmetric conducting airways (Zhang and Finlay (2005)).

This thesis explains the development and validation of idealized pediatric upper conducting airways that mimic central conducting airways aerosol deposition in the child conducting airways. An idealized geometry representing the pediatric conducting airways

(from trachea to approximately the third airway bifurcation) was developed with the aim of mimicking the average total deposition of aerosols in these conducting airways.
Accurate and realistic airway replicas of the conducting airways showed that the real conducting airways are an arrangement of asymmetrical bent tubes. Most of the flow ventilation engineering models were developed for symmetrical circular pipes (Pedley et al. (1970)). It is experimentally challenging and expensive to measure ventilation distribution *in vivo* in the human respiratory tract. Instead, application of analytical engineering models to predict inhalation flow characteristics (pressure drop and ventilation distribution) in realistic 3D airway replicas is feasible (van Ertbruggen et al. (2005)). Comparing the analytical engineering model that was applied in predicting ventilation distribution in the human lung to *in vitro* experimental data provides a logical method in assessment of respiratory tract function (Ismail et al. (2013)).

Due to resolution limits of CT-scanner cameras, currently it is difficult to capture and segment the distal airway generations of the human lung (Ismail et al. (2013)). Therefore, there is a need to adopt a mathematical model in order to predict flow characteristics in the distal human respiratory tract. Recently, a significant number of studies have used analytical models of the human respiratory tract to investigate particle deposition in different regions of the lung (Taulbee & Yu (1975); Phalen et al. (1985); Hofmann et al. (1989); Yu et al. (1992); Darquenne & Paiva (1994); Asgharian et al. (2001)), gas mixing (Scherer et al. (1972); Chang & Farhi (1973); Pack et al. (1977); Paiva & Engel (1979); de Vries et al. (1981); Verbanck & Paiva (1990)) and flow distribution (Gillis & Lutchen (1999); Katz et al.(2011); Swan et al. (2012); Gouinaud et al. (2014)).

An additional aim of this thesis is to describe research performed toward developing and validating engineering analytical models that predict airway resistance in realistic multiple-path replicas of the human conducting airways.

1.3 Research outline

This thesis consists of six chapters. Chapter 1 presents a short introduction. Chapter 2 continues with a more detailed description of the aerosol deposition in lung airway

replicas digitally reconstructed from CT-scans. The experimental setup that was applied to measure particle deposition in the anatomically accurate airway replicas is described in this chapter. Chapter 3 describes development of an idealized branching airway geometry that mimics average aerosol deposition in pediatric central conducting airways. Chapter 4 describes validation of airway resistance models in predicting pressure drop through anatomically accurate conducting airway replicas for adults and children. The physical airway casts were used to validate the applicability of the analytical correlations for various inhalation flow rates. To obtain a deeper insight into the applicability of the mathematical equations in predicting pressure drop through the conducting airways, the current experimental results have been presented and compared with the data obtained from several analytical models. The main beneficial feature of the mathematical model is the application of these models in predicting airway resistance in the realistic airway replicas. Chapter 5 investigates particle deposition in intrathoracic conducting airways using a commercial pressurized metered dose inhaler (pMDI). Lastly, conclusions and suggested future works are given in Chapter 6.

1.4 References

Asghrian, B., W. Hofmann and R. Bergmann. Particle deposition in a multiple-path model of the human lung. *Journal of Aerosol Science and Technology*. 34:332-339, 2001.

Below, A., D. Bickmann and J. Breitkreutz. Assessing the performance of two dry powder inhalers in preschool children using an idealized pediatric upper airway model. *International Journal of Pharmaceutics*. 444:169-174, 2013.

Bickmann, D., H. Wachtel, R. Kroger and P. Langguth. Examining inhaler performance using a child's throat model. *Respiratory Drug Delivery*. 2:565-570, 2008.

Bowes III S. M. and D. L. Swift. Deposition of inhaled particles in the oral airway during oronasal breathing. *Journal of Aerosol Science and Technology*. 11(2):157-167, 1989.

Briant J. K. and B. S. Cohen. Flow distribution through human and canine airways during inhalation and exhalation. *American Physiological Society,* 67(4): 1649-1654, 1989.

Byron, P. R., M. Hindle, C. F. Lange, P. W. Longest, D. McRobbie, M. J. Oldham, B. Olsson, C. G. Thiel, H. Wachtel and W. H. Finlay. *In vivo-In vitro* correlatins: Predicting

pulmonary drug deposition from pharmaceutical aerosols. *Journal of Aerosol Medicine and Pulmonary Drug Delivery*. 23 (Suppl 2):S59-S69, 2010.

Cheng, H. K. and L. E. Farhi. On mathematical analysis of gas transport in the lung. *Journal of Respiration Physiology*. 18:370-385, 1973.

Cheng, K. H. and D. L. Swift. Calculation of total deposition fraction of ultrafine aerosols in human extrathoracic and intrathoracic regions. *Journal of Aerosol Science and Technology*. 22:194-201, 1995.

Chua H. L., G. G. Collis, A. M. Newbury, K. Chan, G. D. Bower, P. D. Sly and P. N. Le Souef. The influence of age on aerosol deposition in children with cystic fibrosis. *European Respiratory Journal*, 7:2185-2491, 1994.

Darquenne, C. J. and M. Paiva. One-dimensional simulation of aerosol transport and deposition in the human lung. *Journal of Applied Physiology*. 77:2889-2898, 1994.

Delvadia, R. R., P. W. Longest and P. R. Byron. *In vitro* tests for aerosol deposition. I: Scaling a physical model of the upper airways to predict drug deposition variation in normal humans. *Journal of Aerosol Medicine and Pulmonary Drug Delivery*. 25:32-40, 2012.

Devadason S. G., M. L. Everard, C. MacEarlan, C. Roller, Q. A. Summers, P. Swift, L. Borgstrom and P. N. Le Souef. Lung deposition from the turbuhaler in children with cystic fibrosis. *European Respiratory Journal*. 10:2023-2028, 1997.

Devadason S. G., T. Huang, S. Walker, R. Troedson and P. N. Le Souef. Distribution of technetium-99m-labelled QVAR ™ delivered using an Autohaler ™ device in children. *European Respiratory Journal*. 21:1007-1011, 2003.

Emmett P. C., R. J. Aitken and W. J. Hannan. Measurements of the total and regional deposition of inhaled particles in the human respiratory tract. *Journal of Aerosol Science,* 13(6):549-560, 1982.

van Ertbruggen, C., C. Hirsch and M. Paiva. Anatomically based three-dimensional model of airways to simulate flow and particle transport using computational fluid dynamics. *Journal of Applied Physiology*, 98:970-980, 2005.

Everard M. L. Radiolabelled deposition studies in childhood. *Thorax*, 49:1259-1266, 1994.

Finlay W. H., L. Golshahi, M. Noga, C. Flores-Mir. Choosing 3-D mouth-throat dimensions: A rational merging of medical imaging and aerodynamics. *Respiratory Drug Delivery 2010*, 1:185-194, 2010.

Gillis H. L. and K. R. Lutchen. How heterogeneous bronchoconstriction affects ventilation distribution in human lungs: A morphometric model. Annals of Biomedical Engineering, 27:14-22, 1999.

Golshahi, L. and W. H. Finlay. An idealized child throat that mimics average pediatric oropharyngeal deposition. *Journal of Aerosol Science and Technology*. 46 :i-iv, 2012.

Golshahi L., M. L. Noga and W. H. Finlay. Deposition of inhaled micrometer-sized particles in oropharyngeal airway replicas of children at constant flow rates. *Journal of Aerosol Science*, 49: 21-31, 2012.

Golshahi L., M. L. Noga, R. B. Thompson and W. H. Finlay. *In vitro* deposition measurement of inhaled micrometer-sized particles in extrathoracic airways of children and adolescents during nose breathing. *Journal of Aerosol Science,* 42(7): 474-488, 2011.

Gouinaud L., I. Katz, A. Martin, J. Hazebroucq, J. Texereau and G. Caillibotte. Inhalation pressure distributions for medical gas mixtures calculated in an infant airway morphology model. Computer Methods in Biomechanic and Biomedical Engineering, 1-9, 2014.

Grgic B., W. H. Finlay, P. K. P. Burnell and A. F. Heenan. *In vitro* intersubject and intrasubject deposition measurements in realistic mouth-throat geometries. *Journal of Aerosol Science*, 35:1025-1040, 2004.

Harrington L., G. Kim Prisk and C. Darquenne. Importance of the bifurcation zone and branch orientation in simulated aerosol deposition in the alveolar zone of the human lung. *Journal of Aerosol Science,*37: 37-62, 2006.

Heyder J., L. Armbruster, J. Gebhart, E. Grein and W. Stahlhofen. Total deposition of aerosol particles in the human respiratory tract for nose and mouth breathing. *Journal of Aerosol Science*, 6:311-328, 1975.

Heyder J., J. Gebhart, G. Heigwer, C. Roth and W. Stahlhofen. Experimental studies of the total deposition of aerosol particles in the human respiratory tract. *Journal of Aerosol Science*, 4:191-208, 1973.

Hofmann, W., T. B. Martonen and R. C. Graham. Predicted deposition of nonhygroscopic aerosols in the human lung as a function of subject age. Journal of Aerosol Medicine, 2:49-68, 1989.

International Commission on Radiological Protection (ICRP). Human Respiratory Tract Model for Radiological Protection. ICRP Publication 66, Pergamon Press, Oxford, 1994.

Ismail, M., A. Comerford and W. A. Wall. Coupled and reduced dimensional modeling of respiratory mechanics during spontaneous breathing. *International Journal for Numerical Methods in Biomedical Engineering*, 29:1285-1305, 2013.

Itoh H., G. C. Smaldone, D. L. Swift, P. O. Alderson and H. N. Wagner. JR. Validation of quantification nuclear imaging for aerosol studies of the lung. *Journal Nuclear Medicine*, 21(6):11, 1980.

Katz I. M., A. R. Martin, P.-A. Muller, K. Terzibachi, C.-H. Feng, G. Caillibotte, J. Sandeau and J. Texereau. The ventilation distribution of helium-oxygen mixtures and the role of inertial losses in the presence of heterogeneous airway obstructions. *Journal of Biomechanics*, 44:1137-1143, 2011.

Kelly, J. T., B. Asgharian, J. S. Kimbell and B. A. Wong. Particle deposition in human nasal airway replicas manufactured by different methods. Part I: Inertial regime particles. *Journal of Aerosol Science and Technology,* 38, 1063-1071, 2004.

Kleinstreuer, C. and Z. Zhang. Targeted drug aerosol deposition analysis for a four-generation lung airway model with hemispherical tumors. Journal of Biomedical Engineering. 125:197-206, 2003.

Kleinstreuer C. and Z. Zhang. An adjustable triple-bifurcation unit (TBU) model for air-particle flow simulations in human tracheobronchial airways. *Journal of Biomechanical Engineering. ASME* 131:021007-1:021007-10, 2009.

Kleinstreuer C., Z. Zhang and J. F. Donohue. Targeted drug-aerosol delivery in the human respiratory system. *Annual Review Biomedical Engineering.* 10:195-220, 2008.

Lambert A. R., P. T. O'Shaughnessy, M. H. Tawhai, E. A. Hoffman and C.-L. Lin. Regional Deposition of particles in an image-based airway model: large-eddy simulation and left-right lung ventilation asymmetry. *Journal of Aerosol Science and Technology,* 45, 11-25, 2011.

Lippmann, M.. Handbook of physiology: section 9: Regional deposition of particles in the human respiratory tract. *Reactions to Environmental Agents*. Lee, D. H. K., H. L. Falk, S. D. Murphy and S. R. Geiger. Eds., 213-232, 1977.

Lippmann, M. and R. E. Albert. The effect of particle size on the regional deposition of inhaled aerosols in the human respiratory tract. *American Industrial Hygiene Association Journal*, 30:257-275, 1969.

Lippmann, M., R. E. Albert, H. T. Peterson and JR. The regional deposition of inhaled aerosols in man. *Inhaled Particles III*, 1:105-120, 1971.

Ma B. and K. Lutchen. An anatomically based hybrid computational model of the human lung and its application to low frequency oscillatory mechanics. *Annals of Biomedical Engineering*. 34: 1691-1704, 2006.

Ma B. and K. Lutchen. CFD simulation of aerosol deposition in an anatomically based human large-medium airway model. *Annals of Biomedical Engineering*. 37: 271-285, 2009.

Martin D. and W. Jacobi. Diffusion deposition of small-sized particles in the bronchial tree. *Health Physics Journal,* 23(1): 23-29, 1972.

McRobbie D. W., S. Pritchard and R. A. Quest. Studies of the human oropharyngeal airspaces using magnetic resonance imaging. I. Validation of a three-dimensional MRI method for producing *ex vivo* virtual and physical casts of the oropharyngeal airways during inspiration. *Journal of Aerosol Medicine,* 16(4): 401-415, 2003.

National Council Radiation Protection Measurement (NCRP). Deposition, retention, and dosimetry of inhaled radioactive substances. *Report No. 125*, Bethesda, MD, 1997.

Newman S. P., G. Woodman and S. W. Clarke. Deposition of carbenicillin aerosols in cystic fibrosis: effects of nebulizer system and breathing pattern. *Thorax*, 43:318-322, 1988.

Oldham M. J., R. C. Mannix and R. F. Phalen. Deposition of monodisperse particles in hollow models representing adult and child-size tracheobronchial airways. *Health Physics*. 72(6): 827-834, 1997.

Pack A., M. B. Hooper, W. Nixon and J. C. Taylor. A computational model of pulmonary gas transport incorporating effective diffusion. Journal of Respiration Physiology. 29:101-124, 1977.

Paiva M. and L. A. Engel. Pulmonary interdependence of gas transport. *Journal of Applied Physiology: Respiratory, Environmental and Exercise Physiology*. 47:296-305, 1979.

Pedley T. J., R. C. Schroter and M. F. Sudlow. Energy losses and pressure drop in models of human airways. *Journal of Respiration Physiology*. 9:371-386, 1970.

Phalen R. F., M. J. Oldham, C. B. Beaucage, T. T. Crocker and J. D. Mortensen. Postnatal enlargement of human tracheobronchial airways and implications for particle deposition. *The Anatomical Record*. 212:368-380, 1985.

Rudolf, G., J. Gebhart, J. Heyder, G. Scheuch and W. Stahlhofen. Mass deposition from inspired polydisperse aerosols. *Annals of Occupational Hygiene*, 32: 919-938, 1988.

Rudolf, G., R. Kobrich and W. Stahlhofen. Modeling and algebraic formulation of regional aerosol deposition in man. *Journal of Aerosol Science,*21(Suppl. 1): S403-S406, 1990.

Rudolf, G., R. Kobrich, W. Stahlhofen and A. C. James. Regional aerosol deposition in man – a statistical and algebraic model. *Annals of Occupational Hygiene*, 38(Suppl. 1): 1-14, 1994.

Scherer P. W., L. H. Shendalman and N. M. Green. Simultaneous diffusion and convection in single breath lung washout. *Bulletin of Mathematical Biophysics Exercise Physiolo*gy. 34(3):393-412, 1972.

Schlesinger, R. B. and M. Lippmann. Particle deposition in casts of the human upper tracheobronchial tree. *American Industrial Hygiene Association Journal*. 33 :237-251, 1972.

Schlesinger, R. B. and M. Lippmann. Selective particle deposition and bronchogenic carcinoma. *Environmental Research*. 15: 424-431, 1978.

Stahlhofen, W., J. Gebhart and J. Heyder. Experimental determination of the regional deposition of aerosol particles in the human respiratory tract. *American Industrial Hygiene Association Journal.* 41(6): 385-398, 1980.

Stahlhofen, W., J. Gebhart and J. Heyder. Biological variability of regional deposition of aerosol particles in the human respiratory tract. *American Industrial Hygiene Association Journal*, 42:348-352, 1981.

Stahlhofen, W., J. Gebhart, J. Heyder and G. Scheuch. New regional deposition data of the human respiratory tract. *Aerosol in Science, Medicine and Technology*, 14(3): 186-188, 1983.

Stahlhofen, W., J. Gebhart, J. Heyder, G. Scheuch and P. Juraske. Particle deposition in extrathoracic airways of healthy subjects and of patients with early stages of laryngeal carcinoma. *The Eleventh Annual Conference of the Association for Aerosol Research*, 15(3):215-218, 1984.

Stapleton K. W., E. Guentsch, M. K. Hoskinson and W. H. Finlay. On the suitability of k-ε turbulence modeling for aerosol deposition in the mouth and throat: a comparison with experiment. *Journal of Aerosol Science.* 31: 739-749, 2000.

Storey-Bishoff, J., M. Noga and W. H. Finlay. Deposition of micrometer-sized aerosol particles in infant nasal airway replicas. *Journal of Aerosol Science.* 39: 1055-1065, 2008.

Svartengren K., P. A. Lindestad, M. Svartengren, G. Bylin, K. Philipson and P. Camner. Deposition of inhaled particles in the mouth and throat of asthmatic subjects. *European Respiratory Journal*. 7: 1467-1473, 1994.

Swan A. J., A. R. Clark and M. H. Tawhai. A computational model of the topographic distribution of ventilation in healthy human lungs. *Journal of Theoretical Biology*. 300:222-231, 2012.

Swift, D. L.. Inspiratory inertial deposition of aerosols in human nasal airway replicate casts: Implication for the proposed NCRP lung model. *Radiation Protection Dosimetry*. 38: 29-34, 1991.

Swift, D. L., Y.-S. Cheng, Y.-F. Su and H.-C. Yeh. Design, characterization and use of replicate human upper airways for radon dosimetry studies. *Indoor radon and lung cancer: Reality or Myth? Part 1.* 26: 213-226, 1992.

Szabo, E. and J. Mulshine. Epidemiology, prognostic factors, and prevention of lung cancer. *Current Opinion in Oncology*. 5(2): 302-309, 1993.

Taulbee D. B. and C. P. Yu. A theory of aerosol deposition in the human respiratory tract. Journal of Applied Physiology. 38:77-85, 1975.

Verbanck S. and M. Paiva. Model simulations of gas mixing and ventilation distribution in the human lung. Journal of Applied Physiology. 69:2269-2279, 1990.

de Vries W. R., S. C. Luijendijk and A. Zwart. Helium and sulfur hexafluoride washout in asymmetric lung models. Journal of Applied Physiology: Respiratory, Environmental and Exercise Physiology. 51:1122-1130, 1981.

Wachtel, H., D. Bickmann, J. Breitkreutz and P. Langguth. Can pediatric throat models and air flow profiles improve our dose ending strategy? *Respiratory Drug Delivery*. 1:195-204, 2010.

Weibel E. R. *Morphometry of the Human Lung.* New York: Academic Press, 1963.

Yu C. P., L. Zhang, M. H. Becquemin, M. Roy and A. Bouchikhi. Algebraic modeling of total and regional deposition of inhaled particles in the human lung of various ages. Journal of Aerosol Science. 23:73-79, 1992.

Zhang, Y. and W. H. Finlay. Experimental measurements of particle deposition in three proximal lung bifurcation models with an idealized mouth-throat. *Journal of Aerosol Medicine*. 18:460-473, 2005.

Zhang Z. and Kleinstreuer C. Effect of particle inlet distributions on deposition in a triple bifurcation lung airway model. *Journal of Aerosol Medicine,* 14(1): 13-29, 2001.

CHAPTER 2 : MEASUREMENTS OF TOTAL AEROSOL DEPOSITION IN INTRATHORACIC CONDUCTING AIRWAY REPLICAS OF CHILDREN

A similar version of this chapter has been published as:

Borojeni, A. A., M. L. Noga, R. Vehring and W. H. Finlay. Measurements of total aerosol deposition in intrathoracic conducting airway replicas of children. *Journal of Aerosol Science*. 73:39-47, 2014.

2.1 Introduction and background

Knowledge of aerosol deposition in human lung airways is essential to evaluate the efficacy of respiratory therapeutic drug delivery during inhalation aerosol therapy for different lung diseases and to investigate the health risks and impacts of inhaled air pollutants and toxicants (Kelly et al., 2004). A large number of studies (see Cheng et al., 1999, 2001; Delvadia et al., 2012; Gurman et al., 1984b; Heenan et al., 2004; Kelly et al., 2004; Lambert et al., 2011; Lin et al., 2001; Liu et al., 2007; Luo & Liu, 2009; Martonen & Lowe, 1982; Oldham et al., 1997; Schlesinger & Lippmann, 1978; Smith et al., 2001; Su & Cheng, 2006; Verbanck et al., 2011; Xi et al., 2011; Yamada et al., 1994; Zhou & Cheng, 2005; also see Zhang & Finlay, 2005a for a review of this literature) have been conducted with engineering models to investigate particle deposition in various regions of the human lung. However, to date only a few quantitative studies have been reported on particle deposition in hollow tracheobronchial casts. Such polymer casts reproduce the real anatomical complexities of the human respiratory tract and mimic the essential parameters affecting aerosol deposition in the different anatomic regions of the human lung (Chan & Lippmann, 1980; Cheng et al., 1999; Grgic et al., 2004b; Gurman et al., 1984a; Schlesinger et al., 1974, 1977, 1982; Schlesinger & Lippmann, 1972, 1976; Storey-Bishoff et al., 2008). More recently, computed tomography (CT) and magnetic resonance imaging(MRI) have provided the capability to generate realistic airway models of different parts of the human respiratory tract (see e.g. Golshahi et al.,2012; Kellyetal., 2004; Lambert et al.,2011; Luo & Liu, 2009; Storey-Bishoff et al.,2008). While a large body of literature has explored deposition of aerosols in airway replicas in adults built using one of the above approaches, few such studies have been performed in child airway replicas. Extrathoracic deposition has been recently characterized in infant and child airway replicas (Golshahi et al.,2011, 2012; Storey-Bishoff et

al.,2008; Zhou et al., 2013a,b) but studies in the tracheobronchial region that would allow general, quantitative, generation-by-generation predictions of pediatric conducting airway deposition are lacking (Oldham et al., 1997). In adults, such empirical correlations are well used in exposure assessment (ICRP,1994) and respiratory drug delivery design (Finlay, 2001). While the extension of adult correlations to predict conducting airway deposition in children has been proposed (Hofmann et al.,1989; ICRP, 1994), validation of such extrapolation remains to be done. In the present work, we measure aerosol deposition in airway replicas of the first few lung generations for 11 children and 5 adults and examine the ability of adult correlations to predict pediatric conducting airway deposition.

2.2 Materials and methods

2.2.1 Airway replicas

This study was approved by the Health Research Ethics Board (HREB) of the University of Alberta. CT scans of subjects who had been imaged for indications other than airway pathology were accessed from archives. A summary of both adult and child subject information is presented in Tables 2.1 and 2.2. Hollow airway replicas of 11 children aged 2–8 years old and 5 adults aged 50–80 years old were built using a rapid prototyping 3-D printer (Invisions SR 3D printer, 3D systems, Rock Hill, SC, USA) in Stereo-Lithography format. The replicas were based on CT scans imaged from each subject's chest in a single helix by a multi-slice CT scanner (Phillips, GEMINI TF TOF16, The Netherlands). A 0.8 mm slice increment thickness (imaging mode was helix and the axial thickness of the reconstructed slices ranged from 0.8 mm to1 mm) was used, as previously described by this research group (Golshahi et al., 2012; Grgic et al., 2004a,b; Storey-Bishoff et al.,2008). The resolution (row × column) of the raw CT images was 512 × 512 pixel. The pixel sizes are in the range of 0.379–0.633 mm, with an average of 0.504±0.072 mm in children and 0.625–0.957 mm, with an average of 0.81±0.088 mm in adults. The CT scan files were recorded in Digital Imaging and Communications in Medicine (DICOM) format. The details of importing CT scan files to the reconstruction software package (MIMICS 3D, Materialise, MI, USA) are explained in more detail elsewhere (Inthavong et al., 2010a,b; Mallepree & Bergers, 2009). Briefly, by selecting a threshold setting defined by a higher and lower bound (min: -1024 and max: -250 in the Hounsfield scale), the airway passage was extracted from the other segmentations. For example, Fig. 2.1 shows the smoothed

segmented bronchial airway of subject8c. The 3D airway models were then converted to stl (Stereo-Lithography) format and exported to the stl editor software package (MAGICS, Materialise, MI, USA) to generate hollow replicate casts with 2 mm outer shell thickness, except subject 3c where the shell thickness was 4 mm. Rapid prototyping was used to generate the airway models from the multi-slice CT images. CT scans were then taken of the built replicas for the assessment of accuracy. Figure 2.2 illustrates both adult and child replicas after building by the 3D printer and prior to testing in the experimental set-up. CT images of each subject's built airway were compared anatomically and dimensionally to the CT images from the actual human subject, with all examined post build dimensions found to differ by less than 5% from the *in vivo* CT dimensions. All replicas include the trachea, main bronchi and airways to the end of generation 3. A summary of the diameters of the airways for each replica, measured from the segmented CT images, is given in Tables 2.1 and 2.2.

Table 2.1: Summary of child subject information and airway diameters of child replicas. Sub. ID# is the subject's identity numbering. Generation 0 (Gen.0) is the trachea, Gen.1 are the main bronchi, Gen.2 are the bronchi and Gen.3 are the segmental bronchi. Stdev is the standard deviation of the range of diameters in each generation.

Age (year)	Subject ID #	Sex	Height (cm)	Weight (kg)	Diameter (stdev) (Gen.0) (mm)	Diameter (stdev) (Gen.1) (mm)	Diameter (stdev) (Gen.2) (mm)	Diameter (stdev) (Gen.3) (mm)
2	8c	F	82	11	5.15(0.24)	4.03(0.06)	3.89(0.36)	2.89(0.73)
4	10c	F	99	16	7.15(0.04)	4.7(1.19)	3.48(0.27)	2.2(0.23)
	14c	F	100	16	7.16(0.15)	6.47(2.77)	4.46(0.69)	2.23(0.76)
5	2c	M	117	22.9	7.05(0.09)	6.03(0.7)	6.00(1.4)	4.35(1.91)
	3c	M	112	20	7.99(0.51)	5.39(0.51)	4.93(0.49)	2.33(0.66)
	9c	M	113	20	7.56(0.01)	6.44(0.87)	5.26(0.01)	3.38(1.05)
6	5c	F	112	18	7.99(0.42)	5.36(1.14)	5.35(1.41)	3.55(1.00)

	6c 12c	F F	118 124	21.5 24	8.5(0.3) 7.41(0.46)	6.75(1.32) 6.45(2.72)	5.94(1.32) 3.28(0.26)	2.9(1.47) 3.23(0.9)
7	13c	F	121	20	9.78(1.32)	7.64(0.09)	6.48(1.23)	3.58(0.01)
8	11c	M	124.5	24.5	10.49(0.95)	7.43(2.26)	6.23(1.42)	3.02(0.35)

Table 2.2: Summary of adult subject information and airway diameters of adult replicas. Column headings are as given in the caption of Table 2.1.

Age (year)	Subject ID #	Sex	Height (cm)	Weight (kg)	Diameter (stdev) (Gen.0) (mm)	Diameter (stdev) (Gen.1) (mm)	Diameter (stdev) (Gen.2) (mm)	Diameter (stdev) (Gen.3) (mm)
50	7a 8a	M F	178 155	113 99	14.57(2.04) 12.4(0.01)	12.34(1.08) 10.83(2.68)	6.79(1.62) 6.53(2.27)	3.6(0.15) 5.18(0.23)
55	3a	F	159	68	14.94(2.67)	14(2.15)	9.45(1.65)	7.46(0.8)
62	4a	M	168	91	14.47(2.09)	13.63(2.5)	7.8(1.04)	4.69(1.04)
80	5a	M	173	76	16.13(2.19)	14.27(2.3)	6.89(2.27)	4.47(1.87)

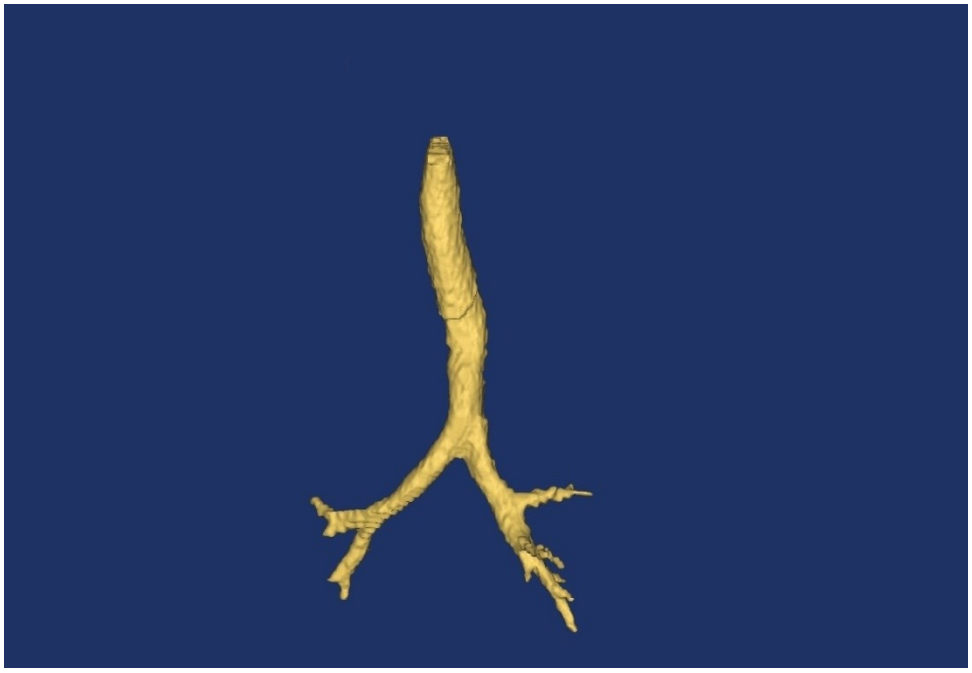

Figure 2.1: Segmentation of the anatomically accurate 3-generation tracheobronchial tree derived from multi-slice CT images of a 2-year-old subject (subject 8c). The tracheobronchial airway was segmented from the CT volumetric data by a threshold algorithm in the range of -250 to -1024 Hounsfield units.

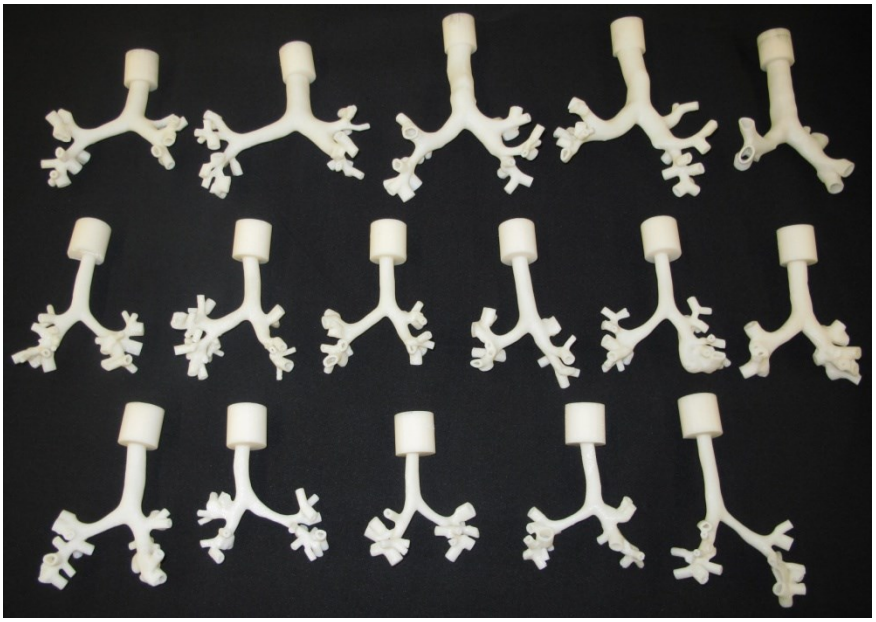

Figure 2.2: 5 anatomically realistic adult hollow tracheobronchial replicas (top row) and 11 anatomically accurate child hollow tracheobronchial replicas (second and third rows)

2.2.2 Experimental set-up and procedure

The experimental set-up includes the equipment depicted schematically in Fig. 2.3. A Condensation Monodisperse Aerosol Generator (CMAG, Model 3475, Topas, Dresden, Germany) generated monodisperse spherical sebacate bis(2-ethylhexyl) (DEHS) (97%, ACROS ORGANICS, AC269920010, USA) oil droplets. These test aerosols were formed by condensation of oil vapor onto NaCl nuclei inside the condensation chimney of the aerosol generator. DEHS particles were selected for the test aerosol because they are stable, nonhygroscopic and spherical under the present experimental conditions.

The generated DEHS particles pass the long path through the generator and condensing tube. Therefore, electrostatically charged particles are neutralized or deposited on the machine and tube walls and the DEHS particles were without significant surface charges (Smaldone et al., 1983).

By changing the operating conditions, particles with diameters in the range of 3.5–5.5 μm were generated and flowed through the airway replica by using a vacuum pump. The generated monodisperse particles were mixed with filtered dilution air via the make-up airline and drawn through the airway replica for less than 1h (exposure time). The duration of exposure time for each replica was determined by the amount of oil that could be held by the replica before overloading and dripping of the replica. The exposure time ranged from 30 min to1h. An Aerodynamic Particle Sizers® (APS™, Model 3321,TSI Inc., MN, USA) was used to monitor the aerodynamic diameter of the droplets and monodispersity during the experimental runs for each test. The measured geometric standard deviation (GSD) of all generated particles in this study was less than 1.22 (GSD <1.22). An aerosol diluter (Model 3302A, TSI Inc., MN, USA) was used with a dilution ratio of 1:100 to dilute the inlet volume flow to be appropriate for the APS. Airway replicas were positioned in an artificial thorax which is a hollow, acrylic plastic, cylindrical chamber. This chamber was sealed at the trachea to provide an air tight respiratory apparatus. The thorax was connected to a vacuum pump through a flexible Teflon tube. Flow rate was adjusted by a digital mass flowmeter (4000 series, TSI Inc., USA) downstream of the replica. The vacuum pump generated steady flow rates (60 and 90 L/min) downstream of the adult replicas and different flow rates in the child replicas were generated to cover the range of physiologically suitable air flow rates inhaled by children listed in the literature (see Table 2.3) (Becquemin et al., 1991, 1999; Chernick et al., 2006; Dozor &Amin, 2002; Hofmann, 1982; Hofmann et al., 1989; ICRP, 1994; Rosenthal & Bush, 2000; Rusconi et al., 1994; Schiller-Scotland et al., 1994a,b; Xu & Yu, 1986).

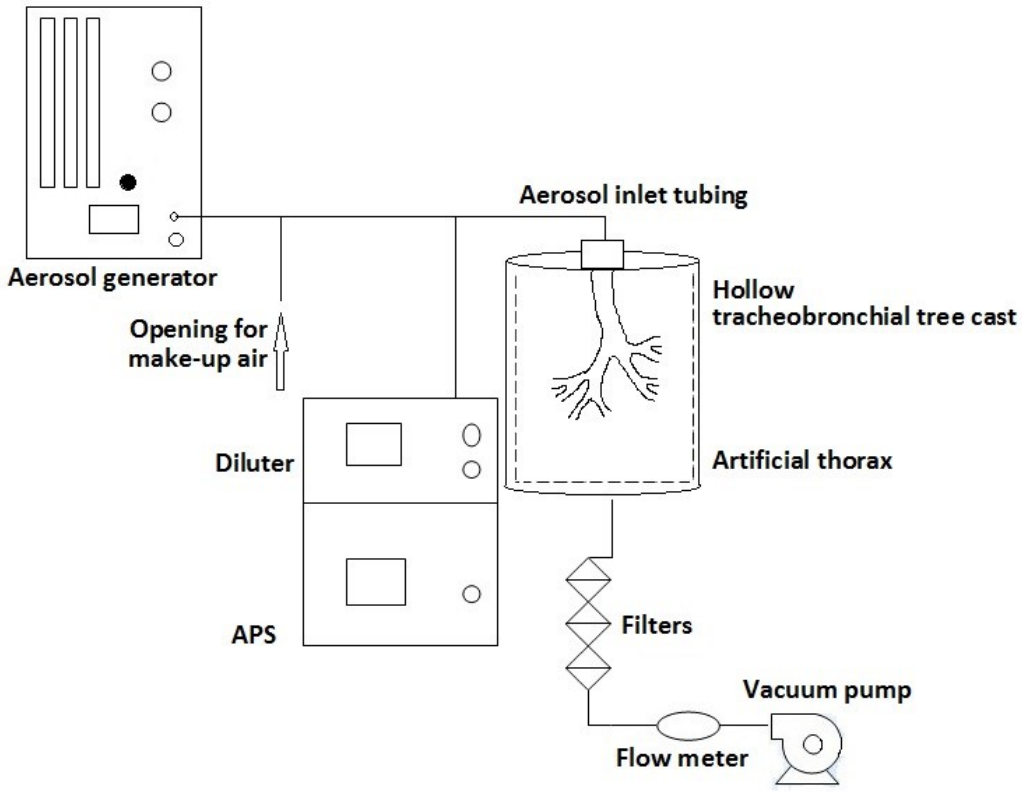

Figure 2.3: Experimental set-up used to measure total particle deposition in realistic child and adult airway replicas. Dashed line indicates paper filters which surrounded the internal surfaces of the artificial thorax.

Table 2.3: Child inspiratory flow rate.

Subject ID #	Tidal Volume, V_T(ml)	Respiration frequency, f_R (breaths/minute)	Average inhalation flow rate, $Q = 2V_T f_R$ (L/min) (Storey-Bishoffetal., 2008)
8c	89.4	26.9	4.8
10c, 14c	152	21.9	6.7
2c, 3c, 9c	181	20.4	7.4
5c, 6c, 12c	209	19.3	8.1

13c	236	18.5	8.7
11c	262	17.8	9.3

A series of 3 runs was carried out at each flow rate. A constant inspiratory flow rate was drawn through the airway replica. The ambient air was entrained through an opening as make-up air to dilute the high concentrated generated particles from the aerosol generator and also provide the desired inhalation flow rate. In this study, total deposition in the hollow replica is defined as

$$\eta_{Total} = \frac{M_m}{(M_m + M_f)} \times 100 \tag{2.1}$$

where M_{m} is the mass of particles deposited in the tracheobronchial airway cast and M_{f} is the mass deposition on all downstream filters (#303 RespirGardII^{TM}, Vital Signs Inc., a GE Healthcare Co., Englewood, CO, USA) including paper filters (Whatmans qualitative paper filter, SIGMA-ALDRICH, USA) which surrounded both the inside and bottom of the artificial thorax. Before weighing the replicas with a calibrated analytical balance (PI-114,Denver Instrument^{TM}, Fisher Scientific, USA) with a resolution of 0.1 mg, the external surface of the trachea bronchial cast was cleaned by paper tissue to remove deposited particles on the outer surfaces.

The casts were weighed before and after wiping the outside of the replicas, with no measureable difference in weight (< 0.001%). Therefore, deposition on the outside of the airway replica is negligible.

The analytical balance accuracy was regularly checked with calibration weights. This gravimetric measurement method has been previously used i n our research lab (Grgic et al.,2004b; Zhang &Finlay, 2005a,b).

2.2.3 Method validation with the existing predictive correlation

The Chan & Lippmann (1980) correlation predicts deposition in each generation, $\boldsymbol{\eta_i}$, where $\boldsymbol{i}$ is the generation number. Total respiratory deposition fraction from the trachea (generation0) to generation 3 inclusive was mathematically calculated as

$$\boldsymbol{\eta_{Total} = 1 - \prod_{i=0}^{3}(1 - \eta_i)}$$

(2.2)

2.3 Results and discussion

In vitro deposition for our five adult airway replicas is shown in Fig. 2.4. Also included in this figure is data from several other published studies, as noted in the figure legend. In the figure are data points where we have used the correlation of Chan &Lippmann (1980) to predict deposition in each airway generation of our subjects, then summed the generational deposition values to give total deposition. As can be seen, good agreement of our data in adult airway replicas with that previously published by others is observed in this figure. The good ability of the Chan & Lippmann (1980) correlation to predict total deposition in our adult airway replicas is seen more clearly in Fig. 2.5, where the data lies close to the line of identity. Figure 2.6 shows total deposition in the child airway replicas. The expected increase in deposition with increasing impaction parameter, $\boldsymbol{d_a^2 Q}$, is observed. However, comparing with Fig. 2.4, it is seen that for a given value of impaction parameter, deposition in our child airway replicas is higher than that in the adult airway replicas. This is expected, due to the smaller airway dimensions of the child airway replicas, and has been noted previously by others (Oldham etal.,1997; Phalen et al.,1988). A comparison of the data in Fig. 2.6 with that published by previous researchers is given in Fig. 2.7. In this figure we have included predictions of deposition in our child airway replicas by using the Chan & Lippmann (1980) correlation to predict airway deposition in each generation within each of our child replicas, and then summing the generational deposition predictions, as noted in Section 2.3, to give total deposition in each of our child replicas. Figure 2.7 shows reasonable agreement of our data compared to that obtained by others. Of considerable interest however is the ability of the Chan & Lippmann (1980) correlation, which is based on adult data, to predict our data. This is seen more clearly in Fig. 8. Despite expected intersubject variability, the Chan & Lippmann (1980) correlation appears to provide reasonably accurate predictions of deposition in our child airway replicas. The usual mechanism for poor predictions from empirical correlations is extrapolation outside the parameter range of the data upon which the correlation was based. Extrapolation of the Chan & Lippmann (1980) correlation from adult to child ages would at first seem to be in this category. However, it must be realized that this correlation, given by $\boldsymbol{\eta = 1.606\, Stk + 0.0023}$ where η is deposition in a given airway generation, depends

only on the Stokes number, Stk, in each airway generation. Particle Stokes number (Stk) is defined as follows:

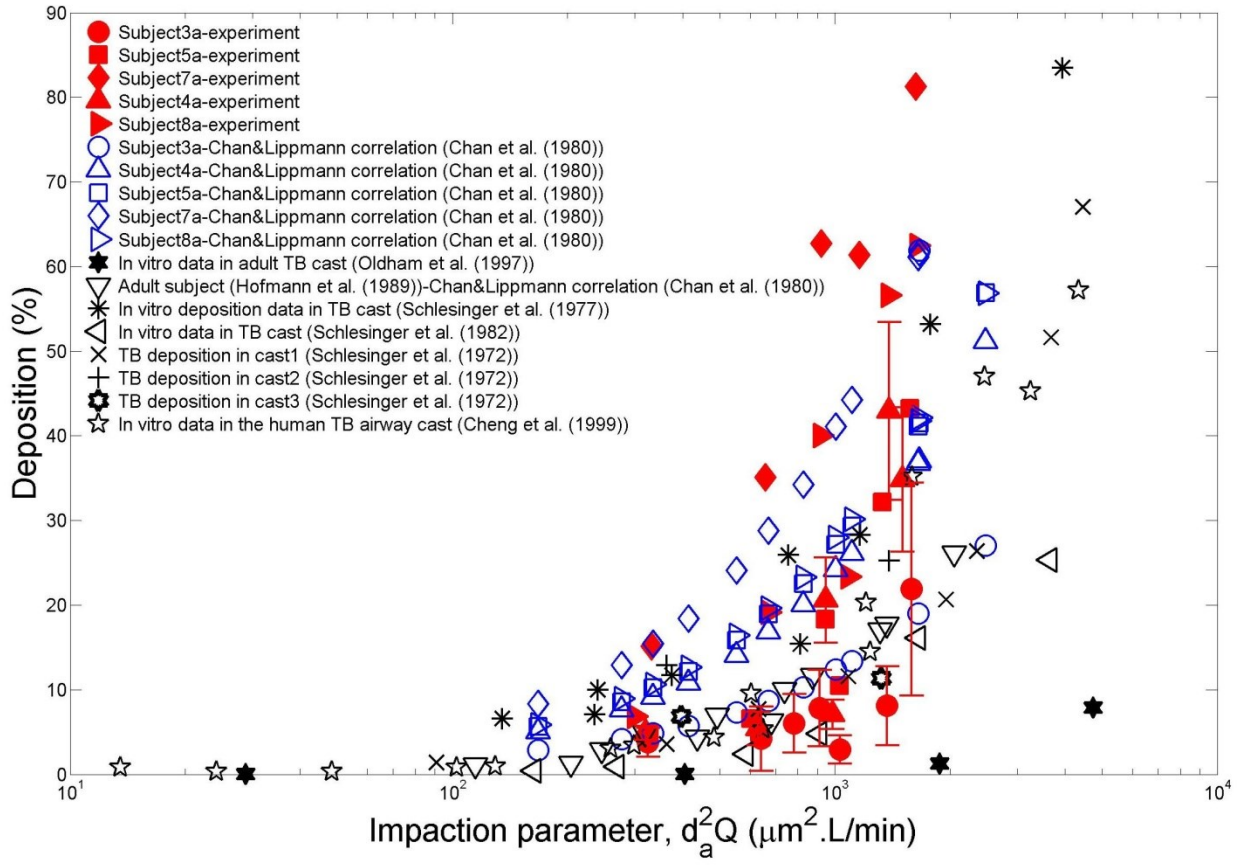

Figure 2.4: *In vitro* intrathoracic airway deposition for adult subjects described in Table 2.2. Each experimental data point is the average of three runs. Error bars indicate standard deviation of the measurements and are smaller than the symbol size for subjects 5a, 7a and 8a.

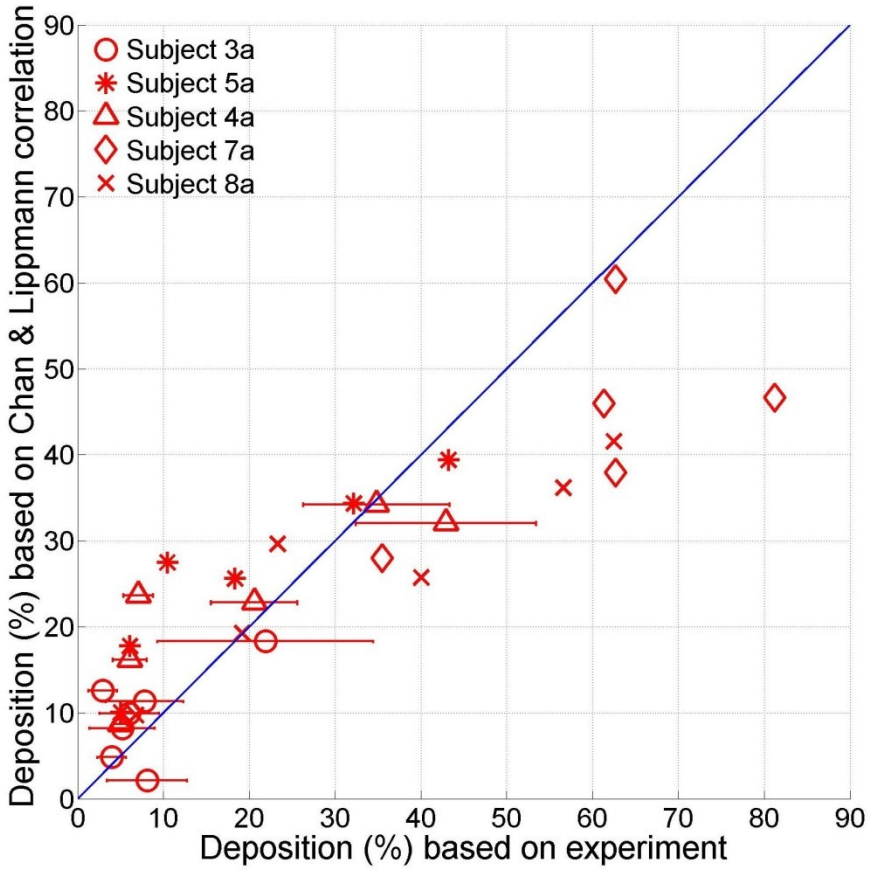

Figure 2.5: Comparison of airway deposition (generation 0–3) based on Chan & Lippmann (1980) correlation with measured experimental total deposition data in our five adult replicas. Each data point is the average of three trials for each experimental condition. Error bars indicate standard deviation of the measurements and are smaller than the symbol size for subjects 5a,7a and 8a.

$$\boldsymbol{Stk} = \frac{\boldsymbol{2\rho_p d_p^2 C_c Q}}{\boldsymbol{9\pi\mu D^3}} \tag{2.3}$$

where $\boldsymbol{\rho_p}$ is the DEHS particle density (=0.912g/cm3), $\boldsymbol{d_p}$ is the particle mass median diameter (MMD), Q is the inhalation flow rate, Cc is the Cunningham slip correction factor (1.03–1.05 for the range of tested particles) and μ is the dynamic viscosity of air. The term $\boldsymbol{\rho_p d_p^2 Q}$ is also known as the inertial parameter. D is the airway generation diameter given in Tables 2.1 and 2.2.

Examination of the Stokes numbers in our experiments reveals that they are similar between our adult and child replicas, as seen in Fig. 2.9, where total deposition in both child and adult airways is plotted vs. Stokes number in the trachea. While Figs. 2.6 and 2.4 show that child airway deposition is higher than adult airway deposition for a given $\boldsymbol{d_a^2 Q}$, Fig. 2.9 shows that the child and adult data collapse together when instead plotted vs. Stokes number, having similar values of Stk between them. Given relatively similar values of Stk between child and adult airway experiments, it is then unsurprising that the adult correlation of Chan & Lippmann (1980) provides reasonable prediction of our data, since use of this correlation in children does not involve extrapolation of Stk, particularly given the larger number of airway generations considered by Chan & Lippmann.

Zhang & Finlay (2005) investigated the effect of the extrathoracic airway including the laryngeal jet on the particle deposition in the bifurcation downstream central conductive airways. Particle deposition in the proximal lung bifurcation model with and without the idealized mouth-throat was measured and compared. This comparison revealed there was only a minor difference between particle deposition in the bifurcation downstream central conductive airways between the two cases (Zhang &Finlay, 2005a). It was concluded, at a steady inspiratory flow rate, the effect of the extrathoracic airway including the laryngeal jet did not affect particle deposition in the bifurcation downstream central conductive airways (Zhang &Finlay, 2005a).

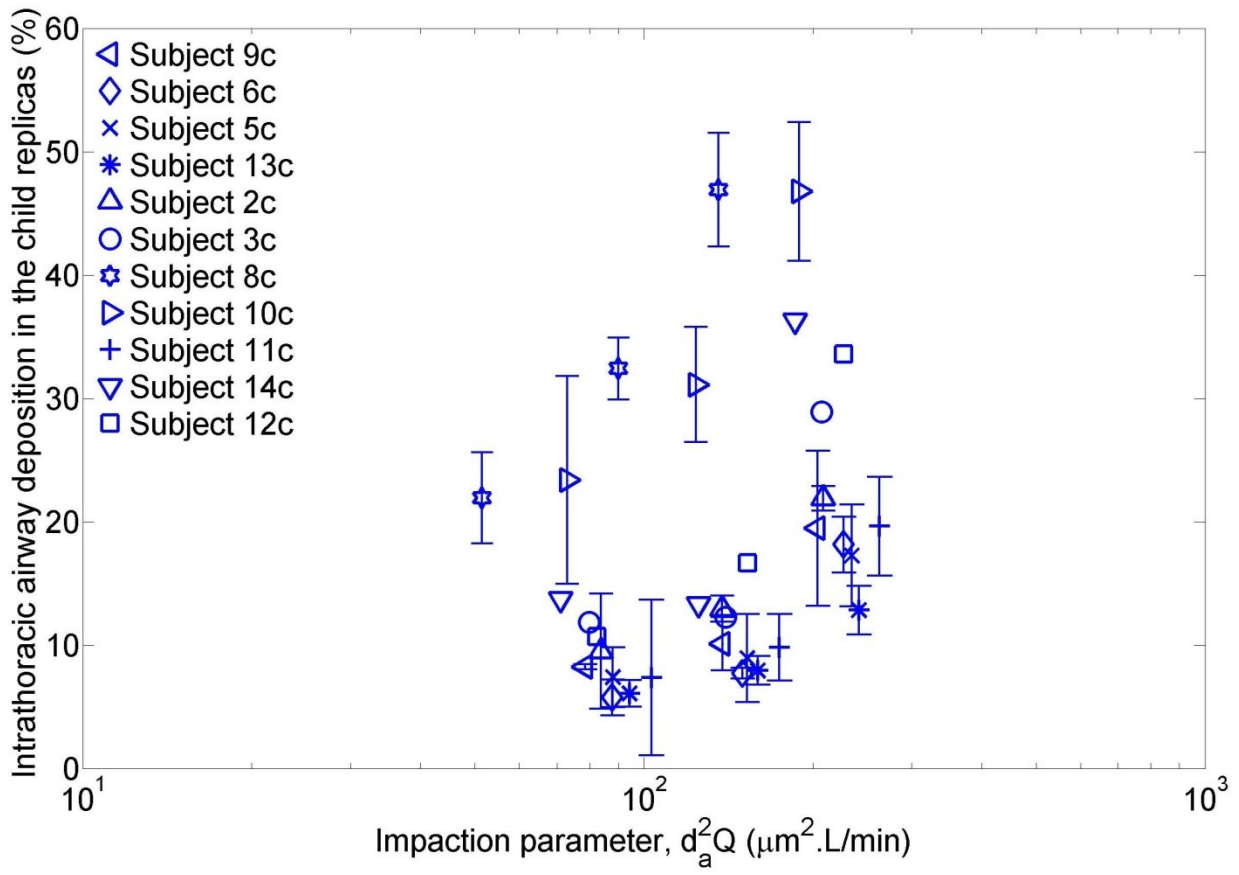

Figure 2.6: Airway deposition (generation 0–3) is shown in the child replicas. Each experimental data point is the average of three runs. Error bars indicate standard deviation of the measurements and are smaller than the symbol size for subjects 3c,12c and 14c.

Given that the Chan &Lippmann (1980) correlation is based on deposition measurements in multiple generations of a single adult cast, intersubject variability and deviation from this correlation would be expected. This is the most obvious explanation for the scatter and deviation of individual data points from the line of identity in Figs. 2.5 and 2.8. It should be noted that with the present experimental setup, flow splitting at each airway branch occurs such that equal pressure drop occurs across each path from the trachea to the exit in to the artificial thorax. *in vivo*, the division of flow at each branch would instead be affected by the volume of the lung branches distal to each airway. Since we have not replicated these distal lung regions, we are of course unable to replicate the actual division of flow in the different airway branches. This limitation of our experimental setup should be borne in mind.

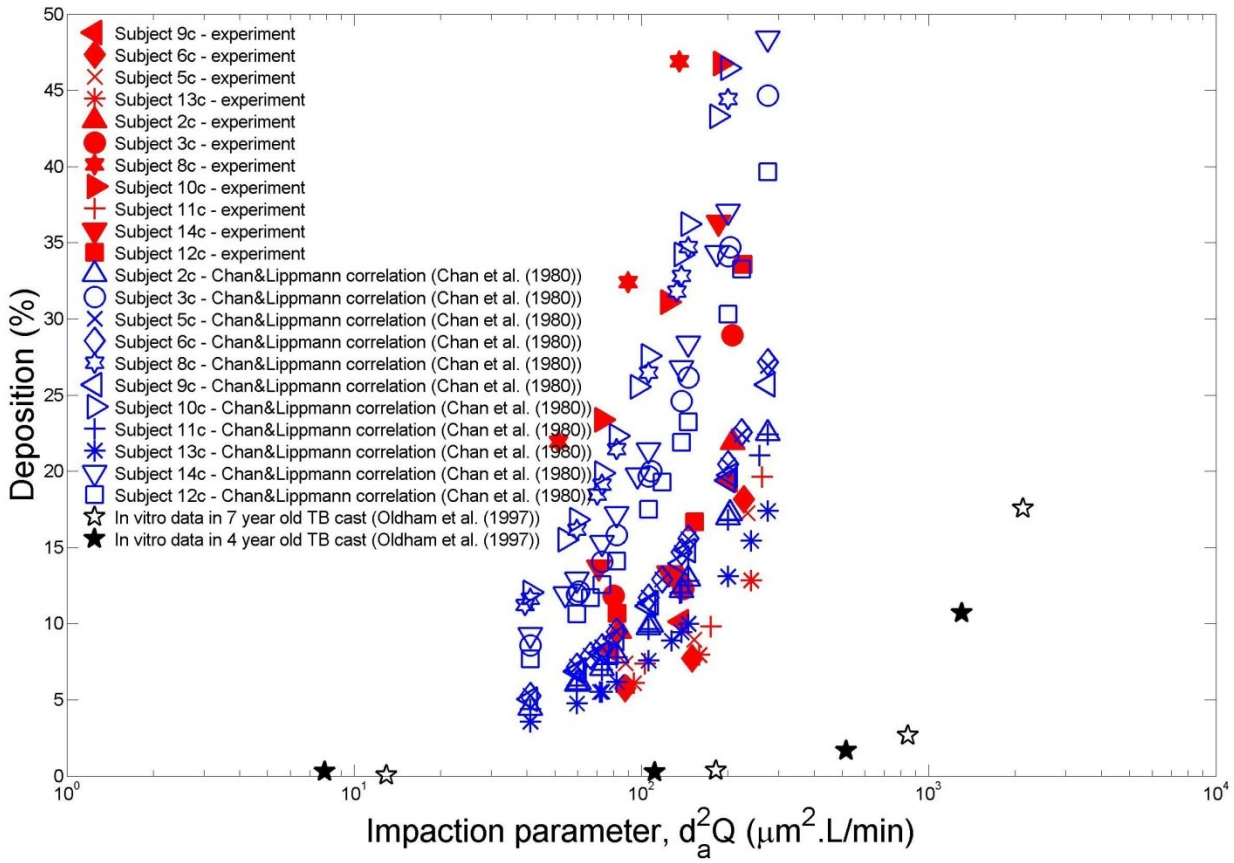

Figure 2.7: *In vitro* intrathoracic airway deposition in child subjects. Each experimental data point is the average of three runs.

2.4 Summary and conclusions

Total deposition was measured in realistic replicas of airway generations 0–3 built from CT scans from eleven children, ages 2–8 years, and five adults. Monodisperse particles with diameters in the range of 3.5–5.5 μm were used to examine total aerosol deposition. While deposition in the child airway replicas is higher than in the adult airway replicas for the same value of the impaction parameter $\boldsymbol{d_a^2 Q}$, they are similar when instead compared at the same Stokes number. Indeed, the data in our child airway replicas is reasonably well predicted by the existing correlation developed for adults by Chan & Lippmann (1980). Researchers interested in predicting deposition in child trachea–bronchial airways thus would appear to be well served, at least for generations 0–3 examined here, by the use of existing Stk-based correlations previously

developed for adult tracheo-bronchial airway deposition, but instead using airway dimensions relevant to children as given by e.g. Hofmann (1982) and Hofmann et al. (1989).

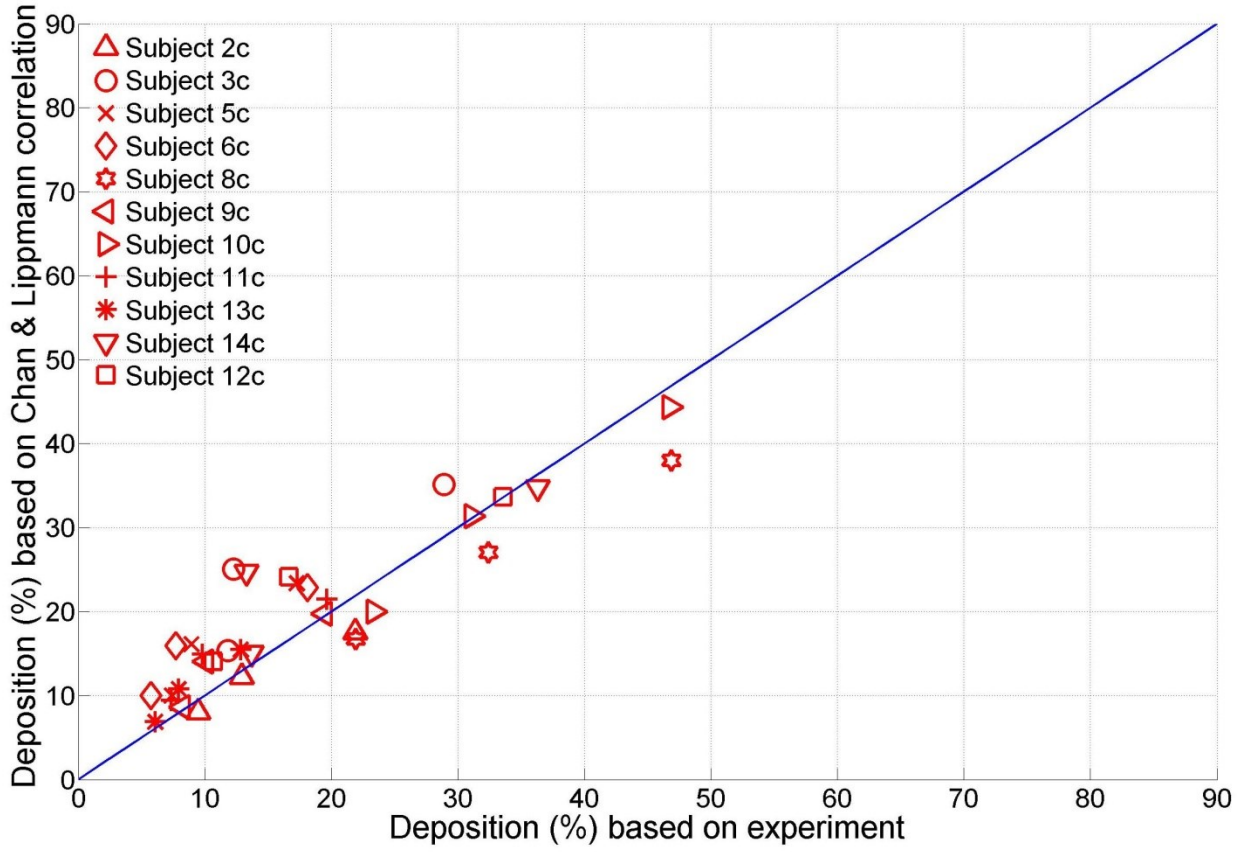

Figure 2.8: Comparison of conducting airway (generation 0–3) deposition based on Chan & Lippmann (1980) correlation with measured experimental total deposition data in child replicas. Each data point is the average of three trials for each experimental condition.

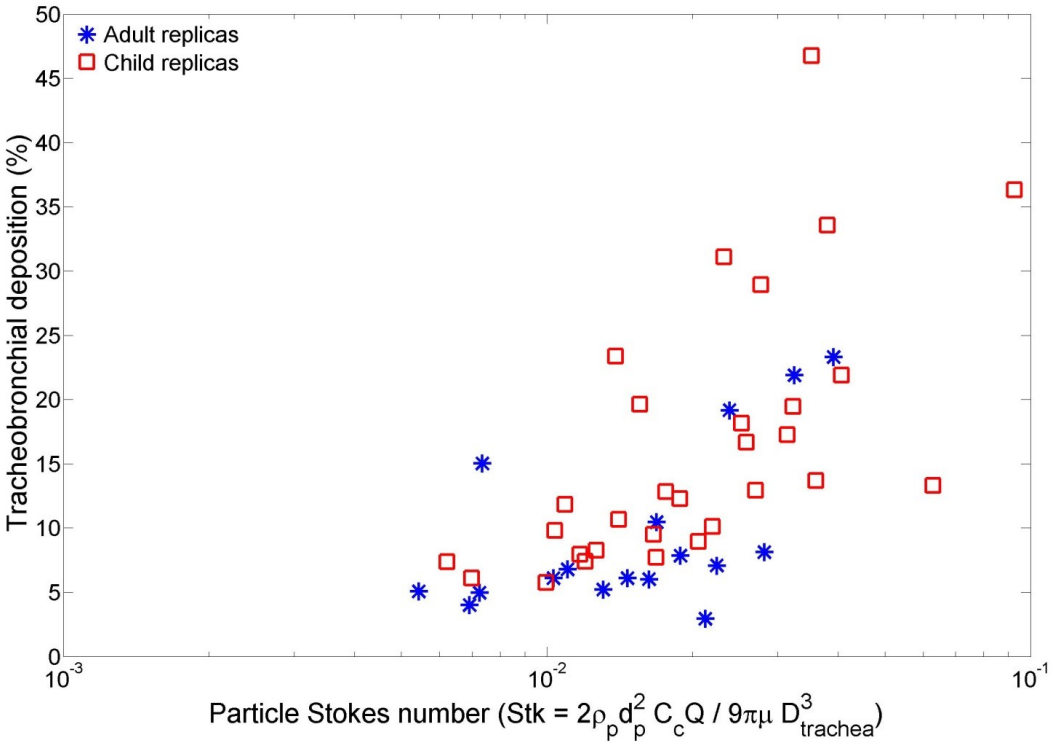

Figure 2.9: Comparison of measured *in vitro* tracheobronchial deposition for the adult subjects with those for the child subjects vs. the Stokes number in the trachea. Each experimental data point is the average of three runs.

2.5 References

Becquemin, M. H., Bertholon, J. F., Bouchikhi, A., Malarbet, J. L., & Roy, M. (1999). Oronasal ventilation partitioning in adults and children: Effect on aerosol deposition in airways. *Radiation Protection Dosimetry Nuclear Technology Publishing*, 81, 221–228.

Becquemin, M. H., Yu, C. P., Roy, M., & Bouchikhi, A. (1991). Total deposition of inhaled particles related to age: Comparison with age-dependent model calculations. *Radiation Protection Dosimetry Nuclear Technology Publishing*, 38, 23–28.

Chan, T. L., & Lippmann, M. (1980). Experimental measurements and empirical modeling of the regional deposition of inhaled particles in human. *American Industrial Hygiene Association Journal*, 41, 399–459.

Cheng, Y. S., Fu, C. S., Yazzie, D., & Zhou, Y. (2001). Respiratory deposition patterns of salbutamol pMDI with CFC and HFA-134a formulations in a human airway replica. *Journal of Aerosol Medicine*, 14, 255–266.

Cheng, Y. S., Zhou, Y., & Chen, B. T. (1999). Particle deposition in a cast of human oral airways. *Aerosol Science and Technology*, 31, 286–300.

Chernick, V., Boat, T. F., Wilmott, R. W., & Bush, A. (2006). *Kendig's Disorders of the Respiratory Tract in Children (Disorders of the Respiratory Tract in Children*) (seventh edition). Saunders: Amsterdam, NL.

Delvadia, R. R., Longest, P. W., Grein, E., & Byron, P. R. (2012). *In vitro* tests for aerosol deposition. I. Scaling a physical model of the upper airways to predict drug deposition variation in normal humans. *Journal of Aerosol Medicine and Pulmonary Drug Delivery*, 25, 32–40.

Dozor, A. J., & Amin, N. (2002). Primary Pediatric Pulmonology. Blackwell Publishing: Hoboken, N J.

Finlay, W. H. (2001). The Mechanics of Inhaled Pharmaceutical Aerosols: An Introduction. Academic Press: Amsterdam, NL.

Golshahi, L., Noga, M. L., & Finlay,W. H. (2012). Deposition of inhaled micrometer-sized particles in oropharyngeal airway replicas of children at constant flow rates. *Journal of Aerosol Science*, 49, 21–31.

Golshahi, L., Noga, M. L., Thompson, R. B., & Finlay, W. H. (2011). *In vitro* deposition measurement of inhaled micrometer-sized particles in extrathoracic airways of children and adolescents during nose breathing. *Journal of Aerosol Science*, 42, 474–488.

Grgic, B., Finlay, W. H., Burnell, P. K. P., & Heenan, A. F. (2004a). *In vitro* intersubject and intrasubject deposition measurements in realistic mouth–throat geometries. *Journal of Aerosol Science*, 35, 1025–1040.

Grgic, B., Finlay, W. H., & Heenan, A. F. (2004b). Regional aerosol deposition and flow measurements in an idealized mouth and throat geometries. *Journal of Aerosol Science*, 35, 21–32.

Gurman, J. L., Lioy, P. J., Lippmann, M., & Schlesinger, R. B. (1984a). Particle deposition in replicate casts of the human upper tracheobronchial tree under constant and cyclic inspiratory flow. II. Empirical model. *Aerosol Science and Technology*, 3, 253–257.

Gurman, J.L., Lippmann, M., & Schlesinger, R.B. (1984b). Particle deposition in replicate casts of the human upper tracheobronchial tree under constant and cyclic inspiratory flow. I. Experimental. *Aerosol Science and Technology*, 3, 245–252.

Heenan, A.F., Finlay, W.H., Grgic, B., Pollard, A., & Burnell, P.K.P. (2004). An investigation of the relationship between the flow field and regional deposition in realistic extra-thoracic airways. *Journal of Aerosol Science*, 35, 1013–1023.

Hofmann, W. (1982). Mathematical model for the postnatal growth of the human lung. *Respiration Physiology*, 49, 115–129.

Hofmann, W., Martonen, T.B., & Graham, R.C. (1989). Predicted deposition of nonhygroscopic aerosols in the human lung as a function of subject age. *Journal of Aerosol Medicine*, 2, 49–68.

ICRP (1994). International Commission on Radiological Protection (ICRP) Publication 66. Human Respiratory Tract Model for Radiological Protection. Pergamon Press: Oxford.

Inthavong, K., Choi, L.-T., Tu, J., Ding, S., & Thien, F. (2010a). Micron particle deposition in a tracheobronchial airway model under different breathing conditions. *Medical Engineering and Physics*, 32, 1198–1212.

Inthavong, K., Tu, J., Ye, Y., Ding, S., Subic, A., & Thien, F. (2010b). Effects of airway obstruction induced by asthma attack on particle deposition. *Journal of Aerosol Science*, 41, 587–601.

Kelly, J. T., Asgharian, B., Kimbell, J. S., & Wong, B. A. (2004). Particle deposition in human nasal airway replicas manufactured by different methods. Part I. Inertial regime particles. *Aerosol Science and Technology*, 38, 1063–1071.

Lambert, A.R., O'Shaughnessy, P.T., Tawhai, M.H., Hoffman,E.A., & Lin,C.-L. (2011). Regional deposition of particles in an image-based airway model: Large- eddy simulation and left–right lung ventilation asymmetry. *Journal of Aerosol Science and Technology*, 45, 11–25.

Lin, T.C., Breysse, P.N., Laube, B.L., & Swift, D.L. (2001). Mouth piece diameter affects deposition efficiency in cast models of the human oral airways. *Journal of Aerosol Science*, 14, 335–341.

Liu, Y., Matida, E.A., Gu, J., & Johnson, M.R. (2007). Numerical simulation of aerosol deposition in a 3-D human nasal cavity using RANS,RANS/EIM, and LES. *Journal of Aerosol Science*, 38, 683–700.

Luo, H.Y., & Liu,Y. (2009). Particle deposition in a CT-scanned human lung airway. *Journal of Biomechanics*, 42, 1869–1876.

Mallepree, T., & Bergers, D. (2009). Complex anatomies in medical rapid prototyping. In: ICBME 2008 (Vol. 23), pp.1866–1869.

Martonen, T.B., & Lowe,J. (1982). Assessment of Aerosol Deposition Patterns in Human Respiratory Tract Casts (Vol. 1). Ann Arbor Science Publishers: Ann Arbor, MI.

Oldham, M.J., Mannix, R.C., & Phalen, R.F. (1997). Deposition of monodisperse particles in hollow models representing adult and child-size tracheobronchial airways. *Health Physics*, 72, 827–834.

Phalen, R.F., Oldham, M.J., Kleinman, M.T., & Crocker, T.T. (1988). Tracheobronchial deposition predictions for infants, children and adolescents. *Annals of Occupational Hygiene*, 32, 11–21.

Rosenthal, M., & Bush, A. (2000). Ventilatory variables in normal children during rest and exercise. *European Respiratory Journal*, 16, 1075–1083.

Rusconi, F., Castagneto, M., Porta, N., Gagliardi, L., Leo, G., Pellegatta, A., Razon, S., & Braga, M. (1994). Reference values for respiratory rate in the first 3 years of life. *Journal of the American Academy of Pediatrics*, 94, 350–355.

Schiller-Scotland, C.F., Hlawa, R., & Gebhart, J. (1994a). Experimental data for total deposition in the respiratory tract of children. *Toxicology Letters*, 72, 137–144.

Schiller-Scotland, C.F., Hlawa, R., Gebhart, J., Heyder, J., Roth, C., & Wonne, R. (1994b). Particle deposition in the respiratory tract of children during spontaneous and controlled mouth breathing. *American Industrial Hygiene Association Journal*, 38, 117–125.

Schlesinger, R.B., Bohning, D.E., Chan, T.L., & Lippmann, M. (1977). Particle deposition in a hollow cast of the human tracheobronchial tree. *Journal of Aerosol Science*, 8, 429–445.

Schlesinger, R.B., Cohen, V.R., & Lippmann, M. (1974). Studies of intrabronchial particle deposition using hollow bronchial casts. In: Experimental Lung Cancer: Carcinogenesis and Bioassays. *International Symposium Held at the Battelle Seattle Research Center*, pp.116–127.

Schlesinger, R.B., Gurman, J.L., & Lippmann, M. (1982). Particle deposition within bronchial airways: Comparisons using constant and cyclic inspiratory flows. *Annals of Occupational Hygiene*, 26, 47–64.

Schlesinger, R.B., & Lippmann, M. (1972). Particle deposition in casts of the human upper tracheobronchial tree. *American Industrial Hygiene Association Journal*, 33, 237–251.

Schlesinger, R.B., & Lippmann, M. (1976). Particle deposition in the trachea: *In vivo* and in hollow casts. *Thorax*, 31, 678–684.

Schlesinger, R.B., & Lippmann, M. (1978). Selective particle deposition and bronchogenic carcinoma. *Environmental Research*, 15, 424–431.

Smaldone, G. C., Itoh, H., Swift, D. L., Kaplan, J., Florek, R., Wells, W., & Wagner, H. N., JR. (1983). Production of pharmacologic monodisperse aerosols. *Appl. Physiol.: Respirat. Environ. Exercise Physiol.*, 54(2), 393–399.

Smith, S.M., Cheng, Y.S., & Yeh, H.C. (2001). Deposition of ultrafine particles in human tracheobronchial airways of adults and children. *Inhalation Toxicology*, 35, 697–709.

Storey-Bishoff, J., Noga, M., & Finlay, W. (2008). Deposition of micrometer-sized aerosol particles in infant nasal airway replicas. *Journal of Aerosol Science*, 39, 1055–1065.

Su, W.C., & Cheng, Y.S. (2006). Deposition of fiber in a human airway replica. *Journal of Aerosol Science*, 37, 1429–1441.

Verbanck, S., Kalsi, H.S., Biddiscombe, M.F., Agnihotri, V., Belkassem, B., Lacor, C., & Usmani, O.S. (2011). Inspiratory and expiratory aerosol deposition in the upper airway. *Inhalation Toxicology*, 23, 104–111.

Xi, J., Si, X., Kim, J.W., & Berlinski, A. (2011). Simulation of airflow and aerosol deposition in the nasal cavity of a 5-year-old child. *Journal of Aerosol Science*, 42, 156–173.

Xu, G.B., & Yu, C.P. (1986). Effects of age on deposition of inhaled aerosols in the human lung. *Aerosol Science and Technology*, 5, 349–357.

Yamada, Y., Koizumi, A., Fukuda, S., Inaba, J., Cheng, Y.S., & Yeh, H.C. (1994). Deposition of ultrafine monodisperse particles in a human tracheobronchial cast. *Annals of Occupational Hygiene*, 38, 91–100.

Zhang, Y., & Finlay, W.H. (2005a). Experimental measurements of particle deposition in three proximal lung bifurcation models with an idealized mouth– throat. *Journal of Aerosol Medicine*, 18, 460–473.

Zhang, Y., & Finlay, W.H. (2005b). Measurement of the effect of cartilaginous rings on particle deposition in a proximal lung bifurcation model. *Aerosol Science and Technology*, 39, 394–399.

Zhou, Y., & Cheng, Y.S. (2005). Particle deposition in a cast of human tracheobronchial airways. *Aerosol Science and Technology*, 39, 492–500.

Zhou, Y., Guo, M., Xi, J., Irshad, H., & Cheng, Y.S. (2013a). Nasal deposition in infants and children. *Journal of Aerosol Medicine and Pulmonary Drug Delivery*, 26, 1–7.

Zhou, Y., Xi, J., Simpson, J., Irshad, H., & Cheng, Y.S. (2013b). Aerosol deposition in a nasopharyngolaryngeal replica of a 5-year-old child. *Journal of Aerosol Science and Technology*, 47, 275–282.

CHAPTER 3 : AN IDEALIZED BRANCHING AIRWAY GEOMETRY THAT MIMICS AVERAGE AEROSOL DEPOSITION IN PEDIATRIC CENTRAL CONDUCTING AIRWAYS

A similar version of this chapter has been submitted as:

Borojeni, A. A., M. L. Noga, A. R. Martin and W. H. Finlay. An idealized branching airway geometry that mimics average aerosol deposition in pediatric central conducting airways. *Journal of Aerosol Science*. xx :xxx-xxx, 2014.

3.1 Introduction

The use of idealized, representative upper airways geometries that mimic average aerosol deposition in various populations has proven indispensable in the development and assessment of devices used to deliver inhaled pharmaceutical aerosols (Below et al. (2013); Bickmann et al. (2008); Byron et al. (2010); Delvadia et al. (2012); Golshahi and Finlay (2012); Longest et al. (2012); Oldham et al. (1997); Wachtel et al. (2010)). Such idealized geometries exist as a result of extensive fundamental investigation of air flow and aerosol deposition in the upper airways (Grgic et al. (2004); Heenan et al. (2003); Zhang et al. (2007); Zhou et al. (2011)). For many pharmaceutical aerosol delivery devices, physical phenomena that can influence upper airways deposition are sufficiently complex to model that *in vitro* testing on the bench top remains commonplace in research and development. Such phenomena include fluidization and deagglomeration of multi-component powders used in dry powder inhalers (DPIs) and rapid deceleration and evaporation of propellant droplet sprays emitted from pressurized metered-dose inhalers (pMDIs). When evaluating aerosol delivery *in vitro* using upper airways geometries, the fraction of active drug penetrating the geometry is commonly interpreted as the lung dose (Borgstrom et al. (2006)). For the vast majority of inhalers in use and in development, the fraction of drug inhaled into the lung and subsequently exhaled is negligible, such that this interpretation is acceptable. Accordingly, current *in vitro* methods using idealized

upper airways geometries permit average *in vivo* total lung dose to be predicted with a reasonable assurance of accuracy.

In addition to the total, aggregate lung dose, for many inhaled drugs the location of deposition *within* the lungs is suspected to influence therapeutic efficacy. Targeting delivery of albuterol to the central conducting airways has been associated with increased bronchodilation in asthmatics (Usmani et al. (2005)), whereas targeting inhaled dornase alfa to the small airways improved treatment response for cystic fibrosis patients (Bakker et al. (2011)). Likewise, phenotypes of COPD and asthma have been characterized by inflammation affecting the small peripheral airways, such that targeting inhaled drugs to small airways has potential to improve treatment (van den Berge et al. (2011); Lahzami et al. (2008); Usmani et al. (2012)). Determining the distribution of lung dose between central and peripheral airways generally requires *in vivo* imaging experiments with radiolabelled formulations, interpretation of *in vivo* pharmacokinetic data, or use of mathematical models or correlations to predict regional lung doses based on aerosol size distributions measured *in vitro*. Unfortunately, *in vivo* approaches are expensive and time-consuming in early development, while the latter approach fails when presented with phenomena or conditions outside the bounds of the model, or outside the range of experimental data from which the correlation was developed.

For adults, idealized geometries representing the central conducting airways, down to the third lung generation, have been developed (Delvadia et al. (2012); Zhang et al. (2005)) and used to predict the regional distribution of aerosols delivered from commercial inhalers (Delvadia et al. (2012)). Though earlier in development than upper airway geometries that terminate at the trachea, these conducting airway geometries offer the potential to distinguish between formulations and devices that preferentially deposit drug in central branching airways versus those for which aerosol predominantly penetrates to the peripheral airways. The emergence of validated, representative conducting airway geometries would present a valuable tool for early-stage development of delivery systems designed to target central or peripheral airway deposition.

To date, equivalent idealized conducting airway geometries for children are not widely available, largely due to limited aerosol deposition data in children's airways upon which to develop and validate such a geometry. In our recent study, aerosol particle deposition

was measured in physical replicas of central conducting airway geometries obtained from segmented computed tomography (CT) scans of school-aged children (Borojeni et al. (2014)). Considerable variation in deposition was observed, due to intersubject variability in airway geometry. This presents a drawback on the use of any single realistic airway replica as representative of a larger population, unless deposition data for that replica are known to lie along a specific percentile within the range of the population data (e.g. the mean).

This article describes the development and validation of a pediatric idealized branching airway geometry. The idealized geometry was designed to yield deposition efficiency over a representative range of flow rates and aerodynamic particle sizes equivalent to the average deposition measured in 10 realistic central conducting airway replicas of children aged 4-8 years (Borojeni et al. (2014)). In addition, the airway resistance of the idealized geometry was compared with that in the realistic replicas, and the correlation between pressure drop across the airways and aerosol deposition therein was investigated.

3.2 Materials and methods

3.2.1 Idealized Model Development

We have recently reported good agreement between aerosol deposition measured in physical replicas of pediatric central conducting airways and analytical predictions made using the Chan and Lippmann (Chan and Lippmann (1980)) correlation, which was originally developed based on experimental measurements of aerosol deposition performed in casts of adult airways. The Chan and Lippmann (Chan and Lippmann (1980)) correlation predicts the deposition efficiency, η, for a given airway generation to be:

$$\boldsymbol{\eta = 1.606}\mathrm{Stk} + \boldsymbol{0.0023} \tag{3.1}$$

where Stk is the particle Stokes number defined as follows:

$$\mathrm{Stk} = \frac{2\rho_p d_p^2 C_c Q}{9\pi\mu D^3}$$

(3.2)

where ρ_p is the aerosol particle density; d_p is the particle diameter; μ is the dynamic viscosity of air; C_c is the Cunningham slip correction factor; D is the airway diameter; and Q is the flow rate of air.

In using equations 3.1 and 3.2 to predict deposition in pediatric airways, size differences between child and adult airways are accounted for through incorporation of airway diameter in the particle Stokes number. The ability of the Chan and Lippmann (Chan and Lippmann (1980)) correlation to predict deposition in pediatric airways suggests that the main geometrical features affecting deposition in child and adult central conducting airways are similar. Consistent with this suggestion, in the present work, an idealized adult geometry previously described by Zhang et al. (Zhang et al. (2005)) was uniformly scaled down to yield an idealized child geometry. The adult model employed by Zhang et al. (Zhang et al. (2005)), referred to by them as the IB model, was based on asymmetrical branching patterns described by Horsfield and colleagues (Horsfield and Cumming (1968); Horsfield et al. (1971)). This model includes the trachea followed by sequentially bifurcating airways down to the third generation (G0-G3). Total airway deposition efficiency in the adult IB model was previously found to lie well within the range of several sets of *in vivo* data measuring tracheobronchial deposition of inhaled aerosols (Zhang et al. (2005)).

In order to determine an appropriate geometric scale factor, least-squares fitting was done to compare predicted deposition in scaled, idealized geometries (done using the Chan and Lippmann (Chan and Lippmann (1980)) correlation) to the average deposition measured in the 10 realistic pediatric airways. That is to say, the scale factor was allowed to vary, and for each value of the scale factor deposition in an associated idealized, scaled geometry was predicted analytically according to the Chan and Lippmann (Chan and Lippmann (1980)) correlation as follows:

$$\boldsymbol{\eta_{\text{total}} = 1 - \prod_{i=0}^{3} (1 - \eta_i)}$$

(3.3)

where η_i is the deposition efficiency calculated for the i^{th} generation. For each generation, η_i was calculated using the average diameter of all airways in that generation.

The scale factor that produced the minimum least-squares difference with average deposition measured in the realistic pediatric airways was selected, and an idealized pediatric airway geometry was built using this scale factor for validation testing as described below. For the present work, the age range for the idealized pediatric geometry was limited to 4-8 years old; therefore, deposition data for one 2-year-old subject from the original data set presented in Borojeni et al. (Borojeni et al. (2014)) was omitted in calculating the average deposition in the realistic replicas.

Once the optimal scale factor was determined, the adult IB model was uniformly scaled down using the Computer Aided Design (CAD) file (SolidWorks ®, Dassault Systemes, Walthm, MA) in conjunction with the Stereo-Lithography (STL) file (MAGICS, Materialise, MI, USA) to be compatible with the three dimensional printing process. The scaled, hollow, idealized child replica was fabricated using a rapid prototyping 3-D printer (Invision ® SR 3D printer, 3D systems, Rock Hill, SC, USA) from acrylonitrile butadiene styrene (ABS) plastic (P430, Stratasys, Eden Prairie, MN).

3.2.2 Idealized Model Validation: Measurement of Particle Deposition

Using a similar experimental set-up as used in our previous study (Borojeni et al. (2014)), a series of deposition measurements was performed in the idealized child conducting airway replica over a range of monodisperse particle diameters of 3.5, 4.5, 5 and 5.2 μm at steady inspiratory flow rate. A constant inspiratory flow of 7.8 L/min was drawn through the idealized child model placed in an-air tight cylindrical chamber. This flow rate is the average of different flow rates that were used with the realistic child replicas in our previous study (Borojeni et al. (2014)).

Figure 3.1 schematically illustrates the experimental approach that was used for measuring total aerosol deposition in the idealized replica. Further details in this regard were presented previously (Borojeni et al. (2014)). In brief, the experimental apparatus included a Condensation Monodisperse Aerosol Generator (CMAG, Model 3475, Topas, Dresden, Germany) to generate monodisperse sebacate Bis(2-ethylhexyl) (DEHS) (97%, ACROS ORGANICS, AC269920010, USA) oil droplets. Monodispersity and aerodynamic diameter of the generated droplets was monitored by an Aerodynamic Particle Sizer (APS, Model 3321, TSI Inc., MN, USA) during the

experiment. The inlet air flow to the APS was diluted by an aerosol diluter (Model 3302A, TSI Inc., MN, USA) with a dilution ratio of 1:100. A vacuum pump was used to provide the constant flow rate. Dilution air was added to provide the desired air flow rate, and a digital mass flow meter (4000 series, TSI Inc., USA) downstream of the thoracic chamber monitored the amount of adjusted inhalation flow rate.

The total deposition for each particle size in the idealized hollow replica is defined as:

$$\eta_{\mathrm{Total}} = \frac{\mathrm{M_m}}{(\mathrm{M_m} + \mathrm{M_f})} \times 100 \tag{3.4}$$

where $\mathrm{M_m}$ is the mass of particles deposited in the idealized airway cast and $\mathrm{M_f}$ is the mass deposition on the paper filters (Whatman ® qualitative paper filter, SIGMA-ALDRICH, USA) covering the internal walls of the artificial thoracic chamber as well as on all downstream filters (#303 RespirGard II™, Vital Signs Inc., a GE Healthcare Co., Englewood, CO, USA). Masses of deposited particles were weighed using a calibrated analytical balance (PI-114, Denver Instrument™, Fisher Scientific, USA) with a resolution of 0.1 mg. All deposition experiments were repeated in triplicate.

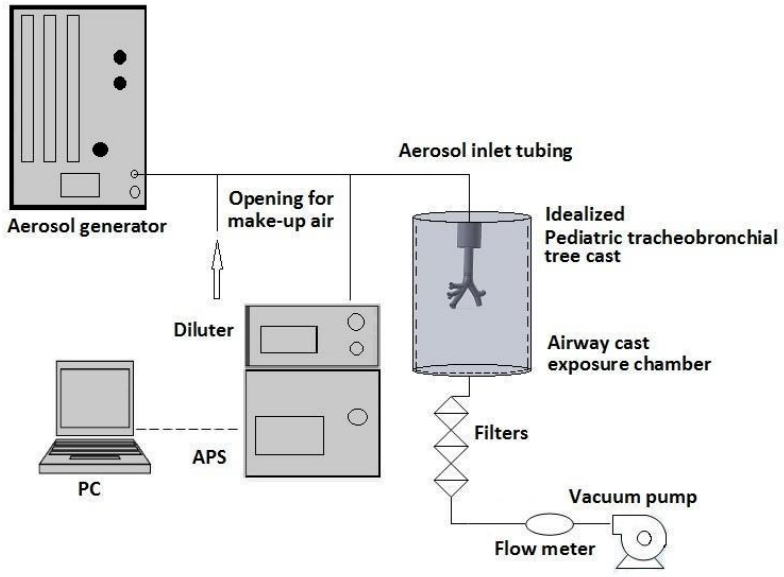

Figure 3.1: Schematic of the experimental apparatus used to measure total particle deposition in the idealized child airway replica. APS = aerodynamic particle sizer.

3.2.3 Measurement of Airway Pressure Drop

The pressure drop across the idealized geometry and across each of the 10 realistic pediatric airway replicas was measured over a range of constant inspiratory flow rates using a low range (0-1.999 inH_2O) digital manometer (HHP- 103, Omega Engineering, Inc., Stamford, CT) with high resolution to 0.001 inH_2O. For each measurement, the idealized geometry or replica was placed in the artificial thoracic chamber, and the pressure was measured at a position downstream from the chamber and upstream from the filters shown in Figure 3.1. Measurements were made a constant flow rates of 2, 5, 10, 15, 20, 30, and 60 L/min. Prior to measurements with the airways in place, the pressure drop across the outlet of the thoracic chamber was measured for each flow rate. This outlet pressure drop was subtracted from measurements made with the airways in place, such that values reported below correspond to a pressure difference between the outside room atmosphere and the negative pressure inside the thoracic chamber. Pressure losses associated with discharge of flow from the airway outlets into the chamber were calculated to be small compared to losses across the airways themselves. Accordingly, reported pressure drops are due to the resistance to flow imposed by the idealized geometry and airway replicas.

3.2.4 Assessment of the Relationship between Deposition and Pressure Drop

In order to assess the correlation between airway resistance and deposition, for each individual airway replica (and for the idealized model) the pressure drop corresponding to each flow rate used in the prior deposition experiments was calculated. This was done by fitting a second order polynomial to the pressure drop versus flow rate data, and then interpolating to determine the pressure drop at other flow rates within the range of experiments. Thereafter, variation in deposition with a modified impaction parameter incorporating pressure drop was assessed with the two parameters determined at equivalent flow rates. Deposition in the airway replicas and idealized model was plotted against the modified impaction parameter $d_a^2 \Delta P$, as previously

considered for nasal aerosol deposition (Garcia et al. (2009); Hounam et al. (1971)), where d_a is the aerodynamic particle diameter. Further, as compared to the parameter $d_a^2 \Delta P$, Garcia et al. (Garcia et al. (2009)) have demonstrated that nasal deposition is more closely correlated with $d_a^2 \Delta P^{2/3}$, where the exponent 2/3 is related to the functional dependence of nasal pressure drop on nasal airway dimensions and flow rate. Similarly, in the present work, a second impaction parameter incorporating ΔP was also evaluated; however, because the influence of airway dimensions and flow rate on pressure drop differs between the nasal and central conducting airways, this parameter differed from that adopted by Garcia et al. (Garcia et al. (2009)). In the Reynolds number range of approximately 100-1000, Pedley et al. (Pedley et al. (1970)) formulated an expression for the ratio between the actual pressure drop through bifurcating airways versus that predicted using the Hagen-Poiseuille equation:

$$Z = \frac{C}{4\sqrt{2}}\left(Re\frac{D}{L}\right)^{1/2} \tag{3.5}$$

where C is a constant determined by the branching angles and parent-to-daughter area ratios of the airways, L is the airway length, and the Reynolds number Re is calculating using the airway diameter D as the length scale.

The pressure drop is then calculated as

$$\begin{aligned} \Delta P &= Z\Delta P_{Hagen-Poiseuille} \\ \Delta P &= Z\frac{128\mu LQ}{\pi D^4} \\ \Delta P &= \frac{64C}{\pi^{1.5}\sqrt{2}}\frac{(\rho\mu L)^{0.5}Q^{1.5}}{D^4} \end{aligned} \tag{3.6}$$

Through comparison with Equation 3.2 for the particle Stokes number, it can be seen by inspection that

$$\text{Stk} \propto \frac{\rho_p d_p^2 Q}{D^3} = \frac{d_a^2 Q}{D^3} \approx d_a^2 \Delta P^{3/4}$$

(3.7)

Accordingly, deposition in the airway replicas and idealized model was also plotted against the modified impaction parameter $d_a^2 \Delta P^{3/4}$ to assess the correlation between this parameter and deposition in central conducting airways.

3.3 Results

3.3.1 Idealized Model Development

A range of geometric scale factors was assessed analytically using equations 3.1-3.3 to predict total deposition in scaled airway replicas. These predictions were compared to the average deposition measured in 10 realistic central conducting airway replicas of children aged 4-8 years old (Borojeni et al. (2014)). Figure 3.2 shows this comparison. A best-fit scale factor of 0.56 was selected based on least-squares fitting to the average data from the realistic replicas.

Figure 3.3 displays the geometry of the idealized model. Dimensions are provided in Table 3.1. Actual sizes in the idealized pediatric central conducting airways geometry are similar to actual geometry diameter measured in 10 realistic replicas.

Table 3.1: Dimensions of the idealized pediatric central conducting airways model

Generation	Length (mm)	Diameter (mm)	Number of airway (s)
0	67.2	8.96	1
1	20.16 (right), 26.88 (left)	6.72	2
2	11.2 (right), 14 (left)	4.2, 3.08, 4.48, 4.48, 4.2	5
3	5.6	2.8, 2.8, 2.8, 2.8, 2.8, 2.8, 3.08, 3.08, 3.08, 3.08	10

3.3.2 Particle Deposition Measurements

Using the optimal scale factor of 0.56 as predicted analytically, an idealized pediatric central conducting airway geometry was built and tested *in vitro*. Figure 3.4 displays the total deposition of particles in the idealized geometry compared to deposition in 10 realistic pediatric airway

replicas for subjects aged 4-8 years old (Borojeni et al. (2014)). It can be observed that the idealized data lie well within the range of the experimental data, and correspond closely with the average deposition data in the 10 realistic replicas.

3.3.3 Airway Pressure Drop

The pressure drop data for constant inspiratory flows of 2, 5, 10, 15, 30 and 60 L/min in the 10 realistic airway replicas, and for the idealized model, are shown in Figure 3.5. The pressure drop across the idealized geometry was found to lie in the lower range of pressure drops measured for the replicas, and was thus lower than the average pressure drop across the replicas.

3.3.4 Deposition vs. Modified Impaction Parameters Incorporating Pressure Drop

Figure 3.6 examines the correlation between deposition in the realistic replicas versus modified impaction parameters that incorporate pressure drop. Best-fit linear least squares correlations relating deposition to the modified impaction parameters are also displayed in Figure 3.6. For comparison, a best-fit linear regression of the traditional impaction parameter d_a^2Q is also shown in Figure 3.6. The correlation based on the parameter d_a^2Q has coefficient of determination (R^2) of 0.20, while that based on $d_a^2\Delta P$ has R^2 =0.45, and that based on $d_a^2\Delta P^{0.75}$ has R^2 = 0.49.

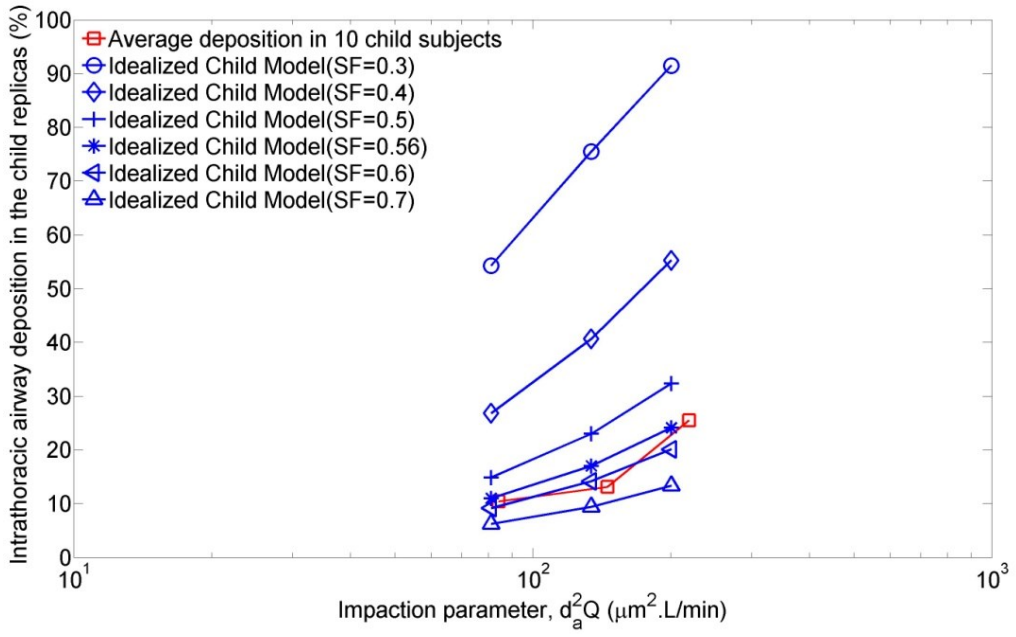

Figure 3.2: Average deposition from 10 child subjects reported by Borojeni et al. (Borojeni et al. (2014)) is plotted against the impaction parameter $d_a^2 Q$, where d_a is the aerodynamic particle diameter and Q is the inspiratory flow rate. In addition, predicted deposition in idealized, scaled geometries is shown, where the scale factor (SF) indicates the isotropic geometric scaling of dimensions from the idealized adult geometry (IB model) presented by Zhang et al. (Zhang et al. (2005)).

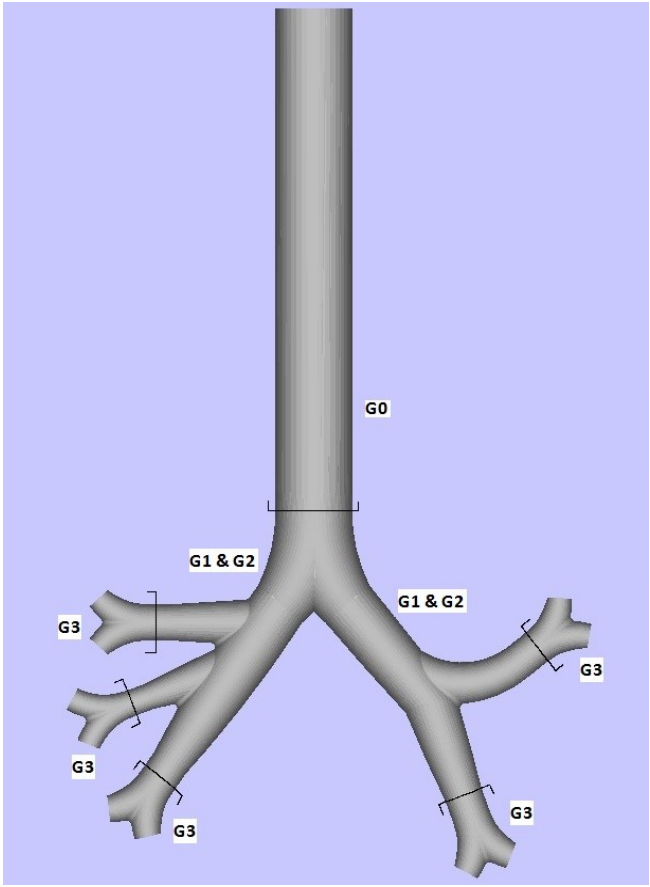

Figure 3.3: Schematic of the idealized pediatric central conducting airways model. Dimensions are provided in Table 3.1. G0, G1, G2 and G3 refer respectively to generation 0 (trachea) through generation 3.

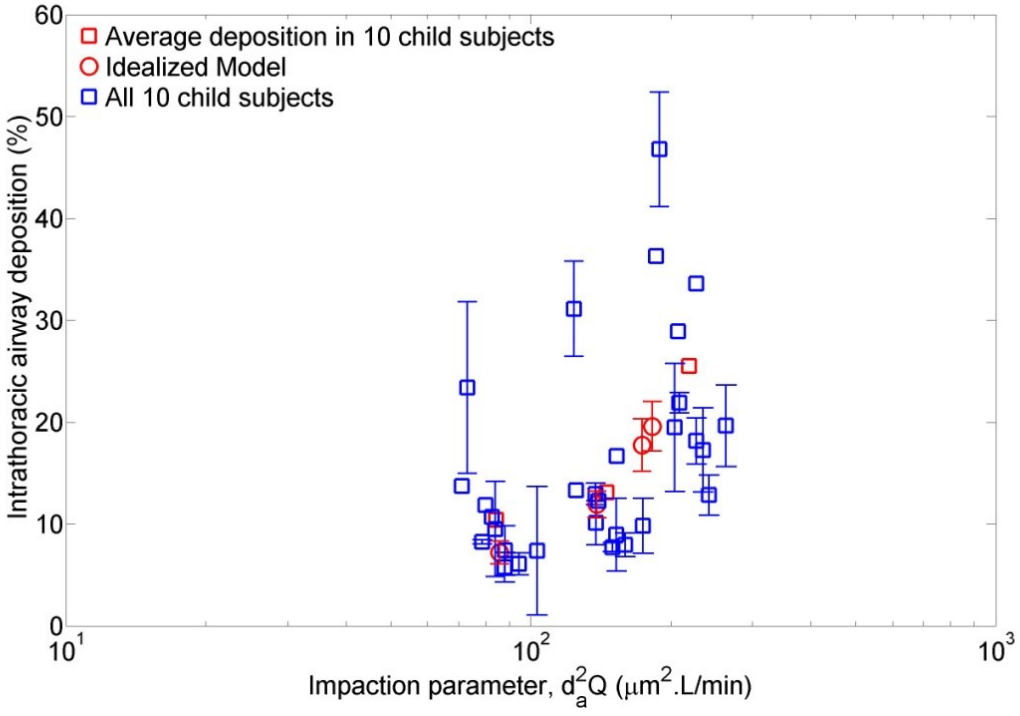

Figure 3.4: Central conducting airway deposition in the idealized pediatric geometry is plotted against the impaction parameter described above for Figure 3.2, and compared to *in vitro* data in 10 realistic pediatric airway replicas for subjects aged 4-8 years old (Borojeni et al. (2014)). Error bars indicate the standard deviation of three replicates. Where error bars are not visible for a data point, they are smaller than the data point in question.

3.4 Discussion

An idealized branching airway geometry has been developed that mimics average aerosol deposition in a subset of pediatric central conducting airway replicas. The geometry was validated through comparison with previous deposition data obtained in 10 realistic airway replicas of children 4-8 years old. The simplified idealized geometry provides several advantages compared with, for example, use of a representative realistic airway selected from the set of 10: all branches within the idealized geometry lie in the same plane, such that the geometry may be manufactured in two, separable halves for inspection and to facilitate chemical assay; the smooth, regular walls of the idealized geometry are less prone to variation resulting from

differences in manufacturing processes between laboratories; and, importantly, the idealized geometry is amenable to manufacture in metal, which permits repeated drug recovery for assay using solvents, and eliminates spurious effects of electric charge on deposition that can occur when some inhalers are used with insulating, plastic airway geometries. The idealized geometry presented herein thus represents a new tool for use in development of pharmaceutical aerosol formulations and delivery devices for school-aged children.

The total deposition in the idealized model represents the deposition in the central conducting airways, from the trachea to the segmental bronchi (generation 3). It does not represent deposition in the whole tracheal-bronchial region of the lung. Accordingly, when coupled with an appropriate upper airways geometry, the fraction of aerosol penetrating the idealized model can be deemed to represent the fraction of aerosol that would penetrate to the lung segments *in vivo*.

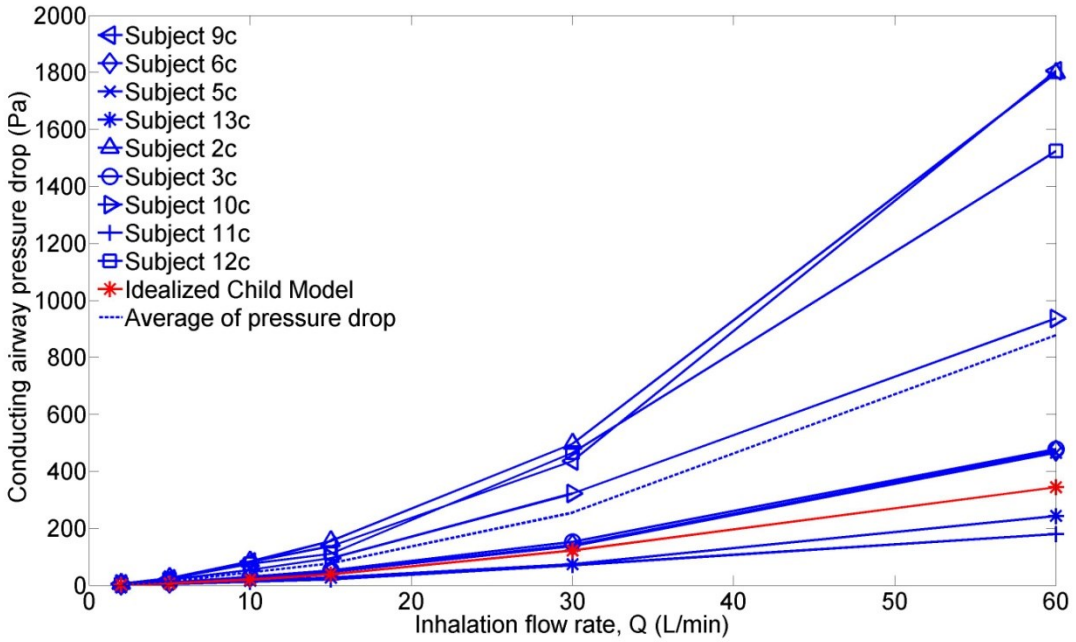

Figure 3.5: Comparison of pressure drop data for inspiratory flows in the realistic replicas with the idealized model.

It is clear from the data presented in Figure 3.5 that the idealized model that mimics average deposition in the realistic replicas does not produce a resistance to flow equivalent to the average in the replicas. Over the range of flow rates tested, the pressure drop across the idealized geometry fell near the lower end of the range of data for the realistic replicas. This result suggests that those geometric features of a branching airway network that most strongly influence aerosol deposition differ from those which determine resistance to flow. Consistent with this hypothesis, incorporation of pressure drop into modified impaction parameters provided only modest collapse of intersubject variability in correlations predicting aerosol deposition as compared to the traditional impaction parameter, $d_a^2 Q$. This is in stark contrast with results for nasal aerosol deposition, in which case use of a modified impaction parameter $d_a^2 \Delta P^{2/3}$ collapsed deposition data tightly around an empirical correlation (Garcia et al. (2009)). While airway deposition and resistance (pressure drop) are both related to underlying airway geometry, their correlation appears to be much weaker in branching central airways than in nasal airways. In the nose and throat, inspiratory flow passing through different sections of the nasal airway including the nasal turbinates and nasopharynx changes direction suddenly. As a result, flow separation may occur, along with its concomitant increase in pressure drop. These same locations of changing flow direction are associated with aerosol deposition, which may explain the observed correlation between aerosol deposition in the nose and throat and transnasal pressure drop (Garcia et al. (2009)). In contrast, there is less logical analogy between central airway deposition and pressure drop. Moving into the lung, continuous energy loss resulting from wall shear stress plays an increasingly dominant role in determining pressure drop, with changes in flow direction at branching points (e.g. the carina) providing only a secondary contribution. This may partly explain why pressure drop and aerosol deposition are not as strongly correlated as in the nose and throat.

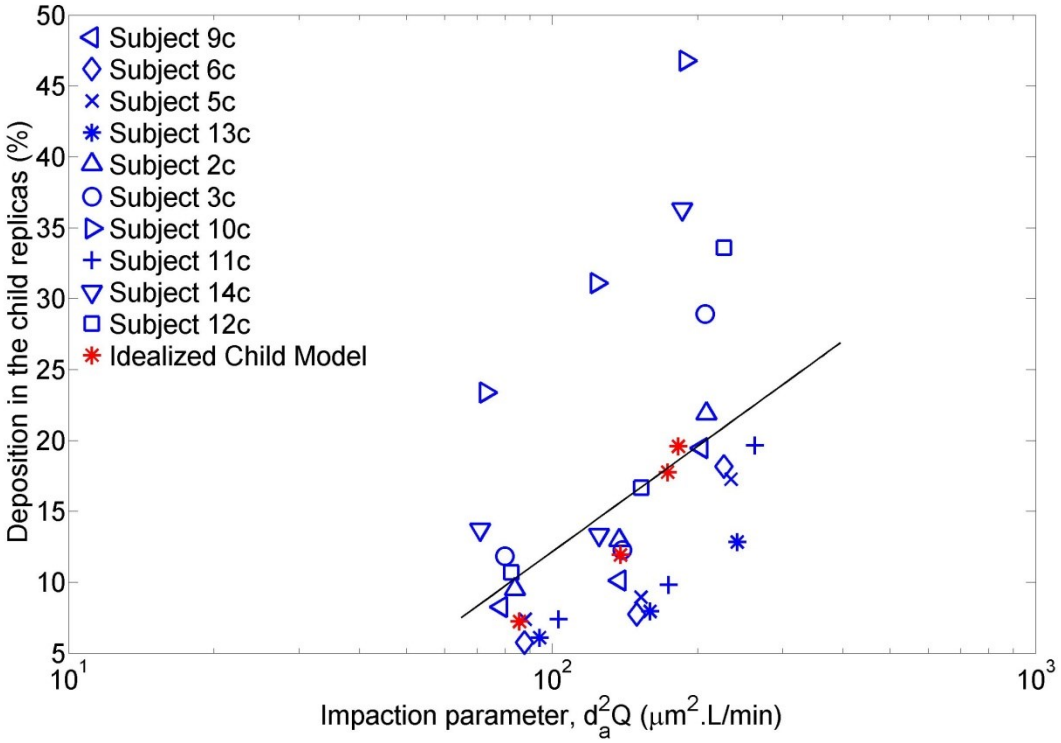

Figure 3.6a: Deposition efficiency in the child replicas and the idealized model as a function of impaction parameter ($d_a^2 Q$). The line is a linear regression least squares fit.

3.5 Conclusions

Experiments confirmed that aerosol deposition in the idealized pediatric central conducting airway geometry was consistent with the average deposition measured in 10 realistic replicas for children 4-8 years old. In contrast, airway resistance in the idealized geometry fell near the lower limit of resistances measured in the realistic replicas, and aerosol deposition was only weakly correlated with pressure drop across the airways. The present idealized geometry represents a tool that may be useful in the research and development of pharmaceutical aerosol delivery to school-aged children.

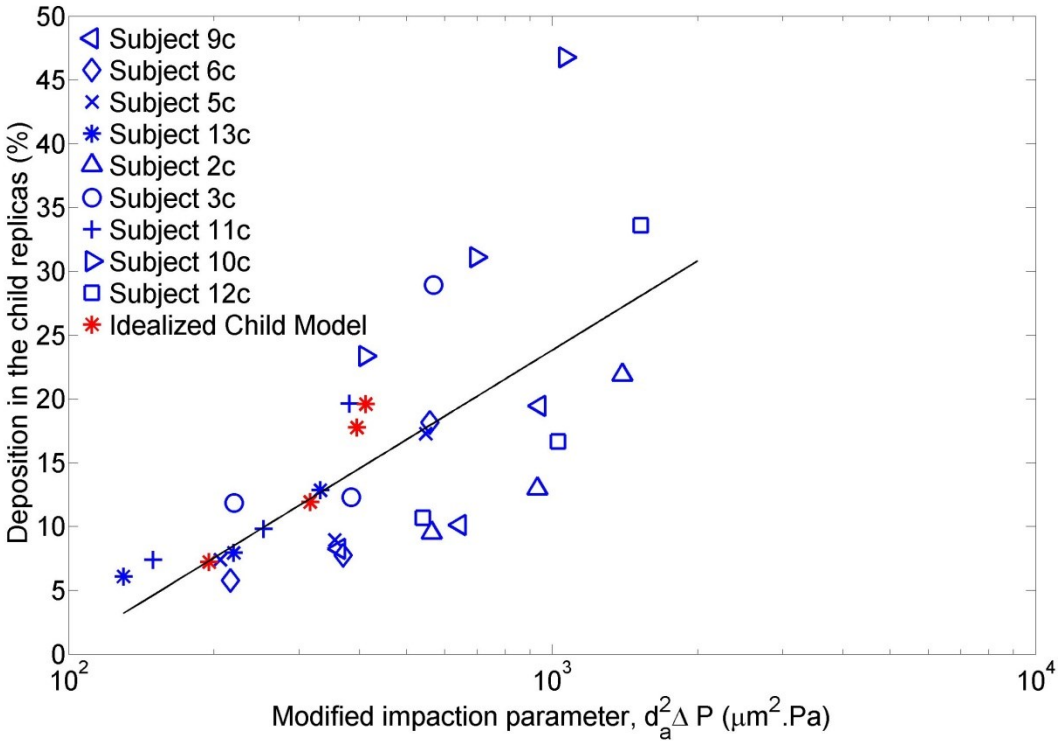

Figure 3.6b: Deposition efficiency in the child replicas and the idealized model as a function of modified impaction parameter ($d_a^2 \Delta P$). The line is a linear regression least squares fit.

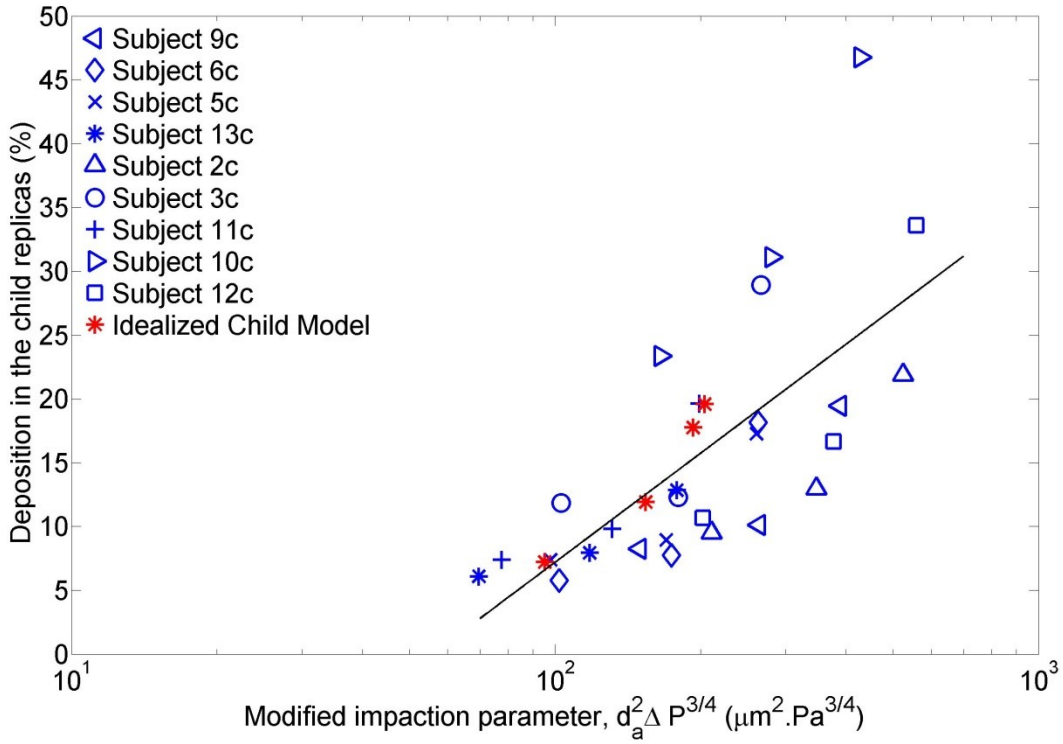

Figure 3.6c: Deposition efficiency in the child replicas and the idealized model as a function of modified impaction parameter ($d_a^2 \Delta P^{3/4}$). The line is a linear regression least squares fit.

3.6 References

Bakker, E. M., S. Volpi, E. Salonini, E. C. van der Wiel-Kooij, C.J.J.C.M. Sintnicolaas, W.C.J. Hop, B.M. Assael, P.J.F.M. Merkus and H.A.W.M. Tiddens. Improved treatment response to dornase alfa in cystic fibrosis patients using controlled inhalation. *European Respiratory Journal*. 38:1328-1335, 2011.

Below, A., D. Bickmann and J. Breitkreutz. Assessing the performance of two dry powder inhalers in preschool children using an idealized pediatric upper airway model. *International Journal of Pharmaceutics*. 444:169-174, 2013.

van den Berge, M., N.H.T. ten Hacken, J. Cohen, W.R. Douma and D.S. Postma. Small airway disease in asthma and copd: clinical implications. *CHEST*. 139:412-423, 2011.

Bickmann, D., H. Wachtel, R. Kroger and P. Langguth. Examining inhaler performance using a child's throat model. *Respiratory Drug Delivery*. 2:565-570, 2008.

Borgstrom, L., B. Olsson and L. Thorsson. Degree of throat deposition can explain the variability in lung deposition of inhaled drugs. *Journal of Aerosol Medicine.* 19:473-483, 2006.

Borojeni, A. A., M. L. Noga, R. Vehring and W. H. Finlay. Measurements of total aerosol deposition in intrathoracic conducting airway replicas of children. *Journal of Aerosol Science*. 73 :39-47, 2014.

Byron, P. R., M. Hindle, C. F. Lange, P. W. Longest, D. McRobbie, M. J. Oldham, B. Olsson, C. G. Thiel, H. Wachtel and W. H. Finlay. *In vivo-In vitro* correlatins: Predicting pulmonary drug deposition from pharmaceutical aerosols. *Journal of Aerosol Medicine and Pulmonary Drug Delivery*. 23 (Suppl 2):S59-S69, 2010.

Chan, T. L. and M. Lippmann. Experimental measurements and empirical modeling of the regional deposition of inhaled particles in human. *American Industrial Hygiene Association Journal*. 41 :399-459, 1980.

Delvadia, R. R., P. W. Longest and P. R. Byron. *In vitro* tests for aerosol deposition. I: Scaling a physical model of the upper airways to predict drug deposition variation in normal humans. *Journal of Aerosol Medicine and Pulmonary Drug Delivery*. 25:32-40, 2012.

Garcia, G. J. M., E. W. Tewksbury, B. A. Wong and J. S. Kimbell. Interindividual variability in nasal filteration as a function of nasal cavity geometry. *Journal of Aerosol Medicine and Pulmonary Drug Delivery*. 22:139-155, 2009.

Golshahi, L. and W. H. Finlay. An idealized child throat that mimics average pediatric oropharyngeal deposition. *Journal of Aerosol Science and Technology*. 46 :i-iv, 2012.

Grgic, B., W. H. Finlay and A. F. Heenan. Regional aerosol deposition and flow measurements in an idealized mouth and throat geometries. *Journal of Aerosol Science.* 35:21-32, 2004.

Heenan, A. F., W. H. Finlay, E. A. Matida and A. Pollard. Experimental measurements and computational modeling of the flow field in an idealized extrathoracic airway. *Experiments in Fluids*. 35:70-85, 2003.

Horsfield, K. and G. Cumming. Morphology of the bronchial tree in man. *Journal of Applied Physiology*. 24 :373-383, 1968.

Horsfield, K., G. Dart and D. E. Olson. Models of the human bronchial tree. *Journal of Applied Physiology*. 31 :207-217, 1971.

Hounam, R. F., A. Black and M. Walsh. The deposition of aerosol particles in the nasopharyngeal region of the human respiratory tract. *Health Physics and Medical Division*. 2 :47-61, 1971.

Lahzami, S. and G. G. King. Targeting d small airways in asthma: the new challenge of inhaled corticosteroid treatment. European Respiratory *Journal.* 31:1145-1147, 2008.

Longest P. W., G. Tian, R. L. Walenga and M. Hindle. Comparing MDI and DPI aerosol deposition using *in vitro* experiments and a new stochastic individual path (SIP) model of the conducting airways. *Pharmaceutical Research*. 29:1670-1688, 2012.

Oldham, M. J., R. C. Mannix and R. F. Phalen. Deposition of monodisperse particles in hollow models representing adult and child-size tracheobronchial airways. *Health Physics*. 72:827-834, 1997.

Pedley, T. J., R. C. Schroter, and M. F. Sudlow. Energy losses and pressure drop in models of human airways. *Journal of Respiration Physiology*. 9: 371-386, 1970.

Usmani, O. S. and P. J. Barnes. Assessing and treating small airways disease in asthma and chronic obstructive pulmonary disease. *Annals of Medicine*. 44:146-156, 2012.

Usmani, O. S., M. F. Biddiscombe and P. J. Barnes. Regional lung deposition and bronchodilator response as a function of beta2-agonist particle size. American Journal of Respiratory and Critical Care Medicine. 172:1497-1504, 2005.

Wachtel, H., D. Bickmann, J. Breitkreutz and P. Langguth. Can pediatric throat models and air flow profiles improve our dose ending strategy? *Respiratory Drug Delivery*. 1:195-204, 2010.

Zhang, Y. and W. H. Finlay. Experimental measurements of particle deposition in three proximal lung bifurcation models with an idealized mouth-throat. *Journal of Aerosol Medicine*. 18:460-473, 2005.

Zhang, Y., K. Gilbertson and W. H. Finlay. In vivo-in vitro comparison of deposition in three mouth-throat models with Qvar ® and Turbuhaler ® inhalers. *Journal of Aerosol Medicine*. 20:227-235, 2007.

Zhou, Y., J. Sun and Y. S. Cheng. Comparison of deposition in the USP and physical mouth-throat models with solid and liquid particles. *Journal of Aerosol Medicine and Pulmonary Drug Delivery*. 24:277-284, 2011.

CHAPTER 4 : VALIDATION OF AIRWAY RESISTANCE MODELS FOR PREDICTING PRESSURE LOSS THROUGH ANATOMICALLY REALISTIC CONDUCTING AIRWAY REPLICAS OF ADULTS AND CHILDREN

A similar version of this chapter has been submitted as:

Borojeni, A. A., M. L. Noga, A. R. Martin and W. H. Finlay. Validation of Airway Resistance Models for Predicting Pressure Loss through Anatomically Realistic Conducting Airway Replicas of Adults and Children. *Journal of Biomechanics*. xx :xxx-xxx, 2014.

4.1 Introduction

Airway resistance is an important parameter used in describing the mechanics of breathing. The relationship between pressure loss and flow rate through the conducting airways influences work of breathing, and is widely used for diagnostic purposes in detecting and classifying respiratory diseases. In addition, variation in airway resistance between individual airways or groups of airways along different paths through the lung plays a role in determining the distribution of ventilation between different lung regions. Ventilation distribution in turn influences regional gas transport, mixing, and uptake, as well as transport and deposition of inhaled aerosols.

Study of the relationship between aggregate pressure loss over the conducting airways dates to the foundational work of Rohrer (Rohrer (1915)). For a given flow rate, the difference in pressure between the airway opening (nose or mouth) and the alveoli was expressed as a summation of linear and quadratic terms, each term weighted by a dimensional constant. Values of these constants varied between subjects, depending on airway dimensions and geometry. The utility of such an approach was clearly demonstrated by Otis and colleagues, who used the Rohrer airway resistance model in combination with experimental measurements to describe, for example, work of breathing (Otis et al. (1950)), ventilation distribution (Otis et al. (1956)), and effects of breathing different gas mixtures on airway resistance (Otis et al. (1949)). These studies provided early insight into the functional relationship between pressure loss, flow rate, gas properties, and airway geometry. However, significant further understanding was gained through fundamental experiments and fluid dynamics analysis performed by Pedley and colleagues (Pedley et al. (1970)). These authors presented an analytical model

of pressure loss through conducting airways of the human bronchial tree based on their measurement of changes to fluid velocity profiles with axial position through idealized, symmetrical airway bifurcations (Pedley et al. (1970)). Pressure loss was found in all cases to exceed that predicted by assuming fully developed Hagen-Poiseuille flow, and an equation was provided through which to calculate the ratio between the actual pressure loss through an airway and that predicted using the Hagen-Poiseuille equation. The magnitude of this ratio varied with airway length and diameter and with the gas Reynolds number (Pedley et al. (1970)).

More recently, computational fluid dynamics (CFD) simulations have been performed to investigate pressure loss through idealized (e.g. Wilquem and Degrez (1997); Comer et al. (2001); Kang et al. (2011); Katz et al. (2011)) and anatomically realistic (e.g. van Ertbruggen et al. (2005); Gemci et al. (2008); Ismail et al. (2013)) adult airway bifurcations. Previous authors have noted that, for adult airways, the Pedley model overestimates their simulated pressure losses (Comer et al. (2001); van Ertbruggen et al. (2005); Katz et al. (2011); Ismail et al. (2013)). Accordingly, alternative analytical models have been proposed (van Ertbruggen et al. (2005); Katz et al. (2011)). In contrast, considerably less work has been done to model airway pressure losses specifically for the conducting airways of children. The accuracy of using analytical models developed based on measurements or simulations performed in adult airway models in predicting pressure loss in children's airways is presently unknown.

In this paper, we describe *in vitro* measurements of the total pressure loss at varying flow rate through anatomically realistic conducting airway replicas of adults and children. The in vitro approach employed presents a unique opportunity to reduce the pressure-flow relationship through the three-dimensional, multi-branching, conducting airway geometry to the classic fluid mechanics problem of flow through a piping network comprising nonlinear resistances (White 2010). Accordingly, analytical predictions of the total pressure loss through the airway replicas made using airway resistance models proposed by Pedley et al. (1970), van Ertbruggen et al. (2005), and Katz et al. (2011) are compared to measured experimental values. Our results are intended to provide guidance for selection of analytical models for use in predicting airway resistance and ventilation distribution in adults and children.

4.2 Methods

4.2.1 Airway Pressure Drop Measurement

Fabrication of realistic adult and child conducting airway replicas has been explained in detail in previous work (Borojeni et al. (2014)). In brief, the conducting airways were identified using Mimics software (MIMICS 3D, Materialise, Ann Arbor, MI, USA) as regions of interest in CT-images of 5 adults and 10 children. Subject information and average airway dimensions are shown in Tables 4.1 and 4.2 for adults and children, respectively. A rapid prototyping technique (Invision® SR 3D printer, 3D systems, Rock Hill, SC, USA) was used to fabricate the conducting airway replicas from acrylonitrile butadiene styrene (ABS) plastic (P430, Stratasys, Eden Prairie, MN).

In the present work, pressure drop across the airway replicas was measured in vitro using a digital pressure gauge (HHP-103, Omega Engineering, Inc., Stamford, CT) with low range (0-498 Pa), high range (0-2590 Pa) and accuracy of ±0.2% full scale. The upstream pressure tap was open to atmosphere and the downstream pressure tap was positioned in the tubing that connected the outlet of an artificial thoracic chamber to a vacuum pump (Figure 4.1). Preliminary measurements were made with the chamber open to characterize the pressure drop across only the chamber outlet at flows ranging from 2 to 90 L/min. Constant flow rates were then drawn through the chamber with the replicas in place by operating a vacuum pump, with flow rates chosen in the range of 15 to 90 L/min for adult replicas and 2 to 60 L/min for child replicas. The desired flow rate was set using a needle valve and monitored by a digital mass flowmeter (TSI Model 4000 series, TSI Inc., Shoreview, MN, USA) downstream of the thoracic cylindrical chamber. The pressure drop across the airway replicas is reported below as the difference between the pressure drop measured with and without the airway replicas in place. Each experimental measurement was repeated three times.

Table 4.1: Summary of adult subject information and airway diameters of adult replicas. Generation 0 (Gen.0) is the trachea, Gen.1 are the main bronchi, Gen.2 are the bronchi and Gen.3 are the segmental bronchi. Stdev is the standard deviation of the range of diameters in each generation (Borojeni et al. (2014)).

Age (year)	Subject Number	Sex	Height (cm)	Weight (kg)	Diameter (stdev) (Gen.0) (mm)	Diameter (stdev) (Gen.1) (mm)	Diameter (stdev) (Gen.2) (mm)	Diameter (stdev) (Gen.3) (mm)
50	7a 8a	M F	178 155	113 99	14.57(2.04) 12.4(0.01)	12.34(1.08) 10.83(2.68)	6.79(1.62) 6.53(2.27)	3.6(0.15) 5.18(0.23)
55	3a	F	159	68	14.94(2.67)	14(2.15)	9.45(1.65)	7.46(0.8)
62	4a	M	168	91	14.47(2.09)	13.63(2.5)	7.8(1.04)	4.69(1.04)
80	5a	M	173	76	16.13(2.19)	14.27(2.3)	6.89(2.27)	4.47(1.87)

Table 4.2: Summary of child subject information and airway diameters of child replicas. Column headings are as given in the caption of Table 1 (Borojeni et al. (2014)).

Age (year)	Subject Number	Sex	Height (cm)	Weight (kg)	Diameter (stdev) (Gen.0) (mm)	Diameter (stdev) (Gen.1) (mm)	Diameter (stdev) (Gen.2) (mm)	Diameter (stdev) (Gen.3) (mm)
4	10c 14c	F F	99 100	16 16	7.15(0.04) 7.16(0.15)	4.7(1.19) 6.47(2.77)	3.48(0.27) 4.46(0.69)	2.2(0.23) 2.23(0.76)
5	2c 3c 9c	M M M	117 112 113	22.9 20 20	7.05(0.09) 7.99(0.51) 7.56(0.01)	6.03(0.7) 5.39(0.51) 6.44(0.87)	6.00(1.4) 4.93(0.49) 5.26(0.01)	4.35(1.91) 2.33(0.66) 3.38(1.05)
6	5c 6c 12c	F F F	112 118 124	18 21.5 24	7.99(0.42) 8.5(0.3) 7.41(0.46)	5.36(1.14) 6.75(1.32) 6.45(2.72)	5.35(1.41) 5.94(1.32) 3.28(0.26)	3.55(1.00) 2.9(1.47) 3.23(0.9)
7	13c	F	121	20	9.78(1.32)	7.64(0.09)	6.48(1.23)	3.58(0.01)
8	11c	M	124.5	24.5	10.49(0.95)	7.43(2.26)	6.23(1.42)	3.02(0.35)

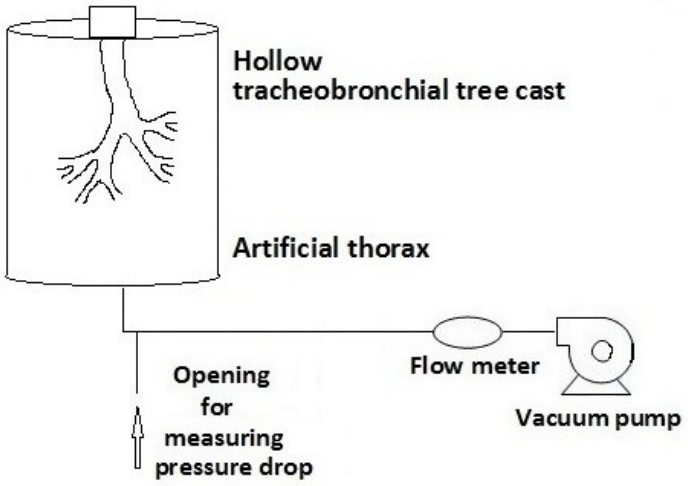

Figure 4.1: Experimental set-up used to measure pressure drop in adult and child CT-based airway replicas.

4.2.2 Analytical Pressure Loss Model

Measured values of pressure drop across the airway replicas were compared with predicted values made using three previously published models of airway resistance (Pedley et al. (1970), (Katz et al.(2011); van Ertbruggen et al. (2005)). For each replica, subject-specific geometry of the conducting airways was required as input in the analytical models of flow distribution and resistance.

4.2.2.1 Determination of Airway Dimensions

Diameters and lengths for all airway segments in each replica were measured from the segmented CT images using a stereolithography (stl) file editor and post processing software package (MAGICS, Materialise, MI, USA). The length of an airway segment was defined as the centerline path length from one bifurcation to the next. The diameter was defined as the average of equivalent cross-sectional area diameters evaluated every 2 mm along the length of the segment.

4.2.2.2 General Solution Procedure

For convenience of calculation, a hydraulic resistance, R, is defined for an airway as

$$R = \frac{\Delta h}{Q^2} \tag{4.1}$$

where Q is the flow rate through the airway and Δh is the head loss, which represents the ratio between pressure drop across the airway (Δp) and fluid density (ρ), i.e. $\Delta h = \Delta p / \rho$. Expressions for the head loss, and consequently resistance, as a function of airway geometry, fluid properties and flow rate result from the application of specific airway resistance models. These will be provided in the following section. At present, the expression given in Equation 1 is used to outline the solution procedure in general. For example, for the simple network of pipes shown in Fig. 4.2 we wish to determine the fraction of the total flow entering airway 0 that flows through each branch, 1a and 1b. To do so, the resistances of branches 1a and 1b must be taken into account, as must be the resistances of all subsequent airway sections downstream. The equivalent hydraulic resistance of either branch can be determined as follows (White (2010)):

$$R_{\text{eq, 1a}} = R_{1a} + \frac{1}{[R_{\text{2aa}}^{-1/2} + R_{\text{2ab}}^{-1/2}]^2} \tag{4.2}$$

$$R_{\text{eq, 1b}} = R_{1b} + \frac{1}{[R_{\text{2ba}}^{-1/2} + R_{\text{2bb}}^{-1/2}]^2} \tag{4.3}$$

In the tracheobronchial tree, the distal airways shown in Figure 4.2 will proceed to bifurcate into further downstream airway generations. In such case it is noted that hydraulic resistances of these downstream airways (i.e. R_{2aa}, R_{2ab}, R_{2ba}, or R_{2bb}) may themselves be expressed as equivalent hydraulic resistance defined using these same principles.

The head loss through any airway branch can then be expressed as

$$\Delta h_n = R_{eq,n} Q_n^2 \tag{4.4}$$

where the equivalent hydraulic resistance $R_{eq,n}$ of that branch is formulated by generalization of equations 2 and 3 and is itself a function of Q_n.

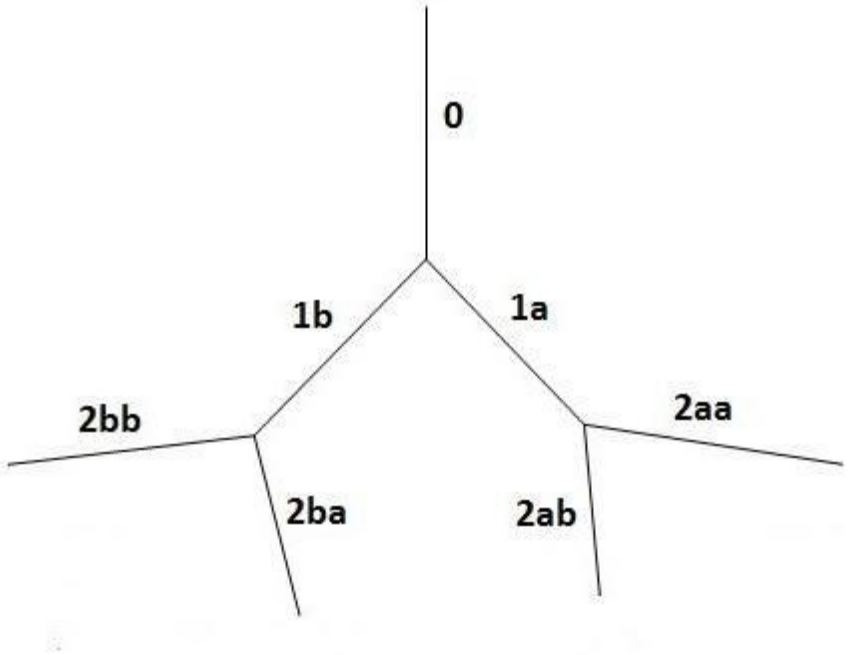

Figure 4.2: Schematic of a simple branching airway network with numbering system used in the analytical model.

Applying this procedure to a branching airway network results in a system of nonlinear algebraic equations. In general for a multiple-path network with *n* paths, a system of *n* equations is obtained. This system of equations can be solved iteratively provided that the head loss is the same across each path. This condition is met in the experiments described above given that all terminal branches supply the artificial thorax chamber. The head loss calculation for each path included a minor loss term accounting for dissipation of kinetic energy due to discharge of flow from terminal branches into the artificial thorax. This term was in all cases small compared with the total head loss across a given path.

The iterative solution procedure starts with an initial guess for the flow rate in each branch. This was made assuming evenly distributed flow between daughter branches at

all bifurcations. The flow rates through each airway branch at subsequent iterations may then be calculated according to:

$$Q_{\mathrm{a}}^{i+1} = \frac{(R_{\mathrm{eq,b}}^{1/2})^{\mathrm{i}}\,(\mathrm{Q_{inlet}})^{i+1}}{[(R_{\mathrm{eq,a}}^{1/2})^{\mathrm{i}} + (R_{\mathrm{eq,b}}^{1/2})^{\mathrm{i}}]} \tag{4.5}$$

where i+1 and i denote the current and previous iteration, respectively, and subscripts a and b indicate daughter airways. Note that equivalent hydraulic resistances are flow rate dependent and thus update on each iteration.

After each iteration, updated flow rates along each path were compared with corresponding values from the previous iteration. The root mean square (RMS) difference in flow rates between successive iterations was used to determine convergence. The solution was deemed converged when this RMS difference fell below 0.006 L/min. The sensitivity of the total head loss to this criterion was trivial for values less than 0.006 L/min. For the converged solution, the total head loss (and corresponding pressure drop) across the airway tree was then calculated using the branch flow rates and resistances.

4.2.2.3 Airway Resistance Models

4.2.2.3.1 Pedley Model

Pedley and colleagues (Pedley et al. (1970)) determined the pressure drop through idealized symmetric models of human bronchial airways based on measurement of changes to inspiratory flow profiles in the streamwise direction. They derived an expression for the ratio relating the actual pressure drop through an airway section to that which would be predicted assuming fully-developed Hagen-Poiseuille flow. This ratio was given by:

$$Z = \frac{1.85}{4\sqrt{2}}\left(Re\frac{D}{L}\right)^{1/2} \tag{4.6}$$

where D and L are airway diameter and length, and Re is the flow Reynolds number:

$$Re = \frac{4Q}{\pi D \nu} \tag{4.7}$$

where ν is the kinematic viscosity of the fluid (air).
The pressure drop is then calculated as:

$$\Delta P_{\text{pedley}} = Z \Delta P_{\text{Hagen-Poiseuille}} \tag{4.8}$$

where,

$$\Delta P_{\text{Hagen-Poiseuille}} = \frac{128 \mu L Q}{\pi D^4} \tag{4.9}$$

where μ is the fluid dynamic viscosity.

Accordingly, the expression for hydraulic resistance, R in a given airway branch for the Pedley model is as follows:

$$R_{\text{pedley}} = \frac{128 \cdot 1.85}{\sqrt{2}\pi^2 D^4} \left(\frac{L}{D}\right)^{0.5} Re^{-0.5} \tag{4.10}$$

where ρ is fluid density.

Note that in analyzing the realistic airway replicas, the value of Z was less than 1 at some distal airways where airway diameter was considerably smaller than the airway length and Reynolds number was small. This is not a physically realistic result as the dissipation of energy in realistic

airways cannot be less than dissipation of energy in the ideal Hagen-Poiseuille flow. Therefore, the value of Z was replaced by 1 in these cases.

It should be noted the Hagen-Poiseuille flow was not directly applied in calculating pressure drop in anatomically accurate child and adult replicas. Poiseuille flow which is a steady, laminar flow in a straight pipe has a parabolic velocity profile. Pedley model was developed as the correction factor of Poiseuille pressure drop based on the property of the Poiseuille flow that the rate of dissipation of energy is minimum (Pedley et al. (1970)). This correction factor was derived as an expression for the ratio relating the actual pressure drop through an airway section to that which would be predicted assuming fully-developed Hagen-Poiseuille flow.

4.2.2.3.2 Modified Pedley Model (van Ertbruggen Model)

van Ertbruggen and colleagues (van Ertbruggen et al. (2005)) used computational fluid dynamics (CFD) to simulate flow through a three-dimensional, anatomically based model of the airways extending from the trachea to the segmental bronchi. This model combined morphometric data data from Horsfield et al. (Horsfield et al. (1971)) with orientation of branching planes based on bronchoscope and CT images. Simulated pressure drop through each airway generation in the model was compared by van Ertbruggen and colleagues (van Ertbruggen et al. (2005)) to values predicted using the Pedley model described above. Pressure drop predicted using the Pedley model was consistently higher than simulated values. The authors therefore proposed a modified form of equation 4.8, as follows:

$$\Delta P_{\text{Pedley}} = \gamma \left(Re \frac{D}{L} \right)^{1/2} \frac{32 \mu L U}{D^2} \tag{4.11}$$

In the original Pedley model (Pedley et al. (1970)) a constant value of $\gamma = 0.327$ was used, consistent with the definition of the correction factor Z provided here in equation 4.6. van Ertbruggen and colleagues (van Ertbruggen et al. (2005)) proposed modified values of γ for each airway generation to better fit their CFD simulation data; values for generations 0-3 are given here in Table 4.3.

Using these values for γ, the expression for hydraulic resistance, R, in a given airway branch for the modified Pedley model is as follows:

$$R_{\text{modified Pedley}} = \frac{512}{\pi^2 D^4}\left(\frac{L}{D}\right)^{0.5}\frac{\gamma}{Re^{0.5}}$$

(4.12)

Table 4.3: Values of the factor γ for different airway generations (van Ertbruggen et al. (2005))

Generation Number	0	1	2	3
Factor γ	0.162	0.239	0.244	0.295

4.2.2.3.3 Katz Model

Katz and colleagues (Katz et al.(2011)) presented a model for calculating pressure drop through the conducting airways based on concepts of major and minor head losses used in engineering analysis of flow through piping networks.

The expression for hydraulic resistance, R, in a given airway branch for the Katz model is as follows:

$$R_{\text{Katz}} = \frac{8}{\pi^2 D^4 g}\left[f\frac{L}{D} + K\right]$$

(4.13)

where f is the friction factor of the pipe. In the Katz model, the friction factor is assumed to be 64/Re for Re < 2000 (laminar flow). Above this value, flow is assumed turbulent and the friction factor is calculated using the correlation derived by Blasius for smooth tubes:

$$f = \frac{0.316}{Re^{0.25}}$$

(4.14)

The minor loss coefficient (K) in Equation 4.13, is calculated using the following correlation developed based on CFD simulations of flow through idealized symmetric airway bifurcations (Katz et al.(2011)):

$$K = \frac{B}{Re^A} + C(\log Re)^2 + D(\log Re) + E \tag{4.15}$$

Values for the constants A through E in Equation 4.15 are provided for generations 0-3 in Table 4.4.

Table 4.4: Values of constants for the minor loss coefficients used in the pressure loss model suggested by Katz and colleagues (Katz et al.(2011))

Number of generation	A	B	C	D	E
0	0.7215	732.9760	-2.3403	19.8089	-42.0336
1	0.4148	4.5209	1.8443	-12.6315	21.9642
2	0.4250	81.3785	-0.0017	2.8211	-12.0867
3	0.7109	94.4163	0.8394	-4.8888	6.8962

4.3 Results

Tracheal Reynolds numbers for adult and child subjects are presented in Table 4.5. At an equivalent volumetric flow rate, Reynolds numbers were higher in child than in adult replicas, owing to the smaller tracheal diameters (and thus higher flow speeds) of the child replicas.

Comparison of measured versus calculated pressure drop through the adult replicas is made in Figures 4.3-4.5 for the three airway resistance models employed. These comparisons indicate there is, in general, reasonable agreement between measured and predicted values, for all three resistance models. It can be further observed that the experimental data are in best agreement with the predicted values made using the modified Pedley (van Ertbruggen et al. 2005) model.

Comparison of measured versus calculated pressure drop through the child replicas is demonstrated in Figures 4.6-4.8. Here the Katz et al. (2010) model and original Pedley et al. (1970) model displayed better agreement with measured values than did the modified Pedley (van Ertbruggen et al. 2005) model, though all three models had a tendency to under predict measured data for the highest measured values of pressure drop, corresponding to higher flow rates through the replicas.

Table 4.5: Values of tracheal Reynolds number at different flow rate in different subjects

Subject ID#	$Re = \frac{4\rho Q}{\pi D_{\text{trachea}} \mu}$						
	Q (L/min) = 2	Q (L/min) = 5	Q (L/min) = 10	Q (L/min) = 15	Q (L/min) = 30	Q (L/min) = 60	Q (L/min) = 90
Subject 3a	---	---	---	1436	2872	5744	8616
Subject 4a	---	---	---	1483	2965	5931	8896
Subject 5a	---	---	---	1331	2661	5322	7984
Subject 7a	---	---	---	1473	2946	5893	8839
Subject 8a	---	---	---	1730	3460	6920	10380
Subject 9c	378	946	1892	2838	5676	11353	---
Subject 6c	337	842	1684	2526	5052	10104	---
Subject 5c	358	895	1790	2685	5371	10742	---
Subject 13c	292	731	1462	2193	4386	8773	---
Subject 2c	406	1014	2029	3043	6087	12174	---
Subject 3c	358	895	1790	2685	5370	10739	---
Subject 11c	273	682	1364	2046	4093	8185	---
Subject 10c	400	1000	2000	3000	6000	11999	---

Subject 12c	386	965	1930	2895	5790	11580	---
Subject 14c	400	999	1998	2997	5993	11987	---

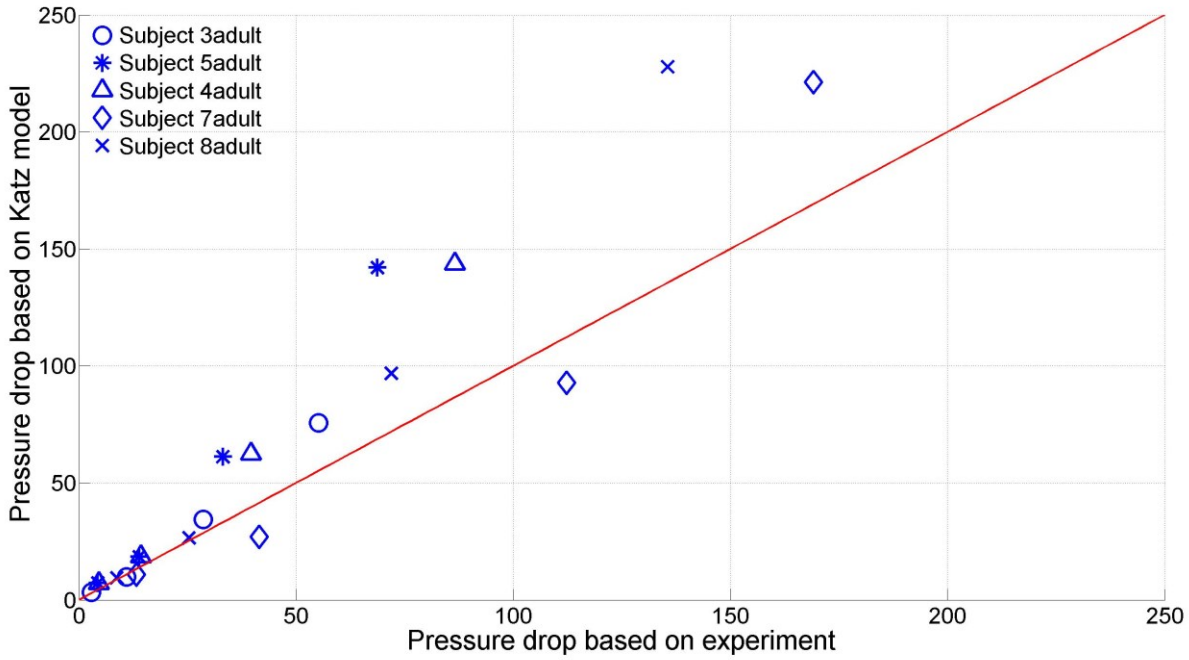

Figure 4.3: Comparison of pressure drop data predicted by Katz et al. (2011) model with the measured data in adult replicas.

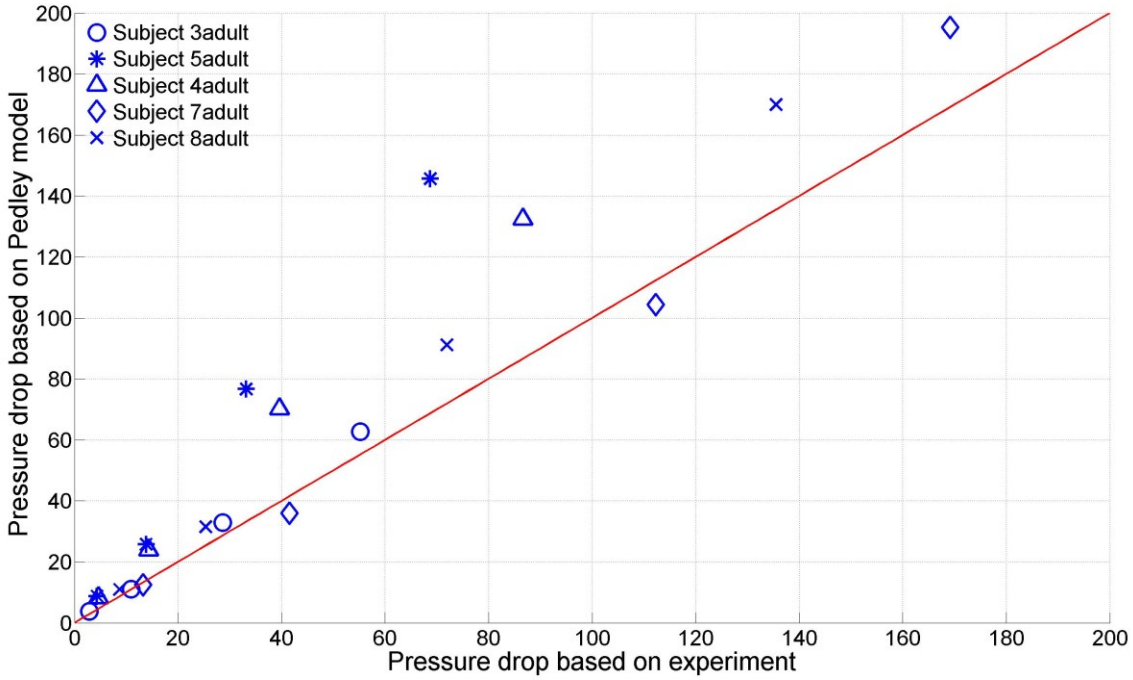

Figure 4.4: Comparison of pressure drop data predicted by the Pedley et al. (1970) model with the measured data in adult replicas.

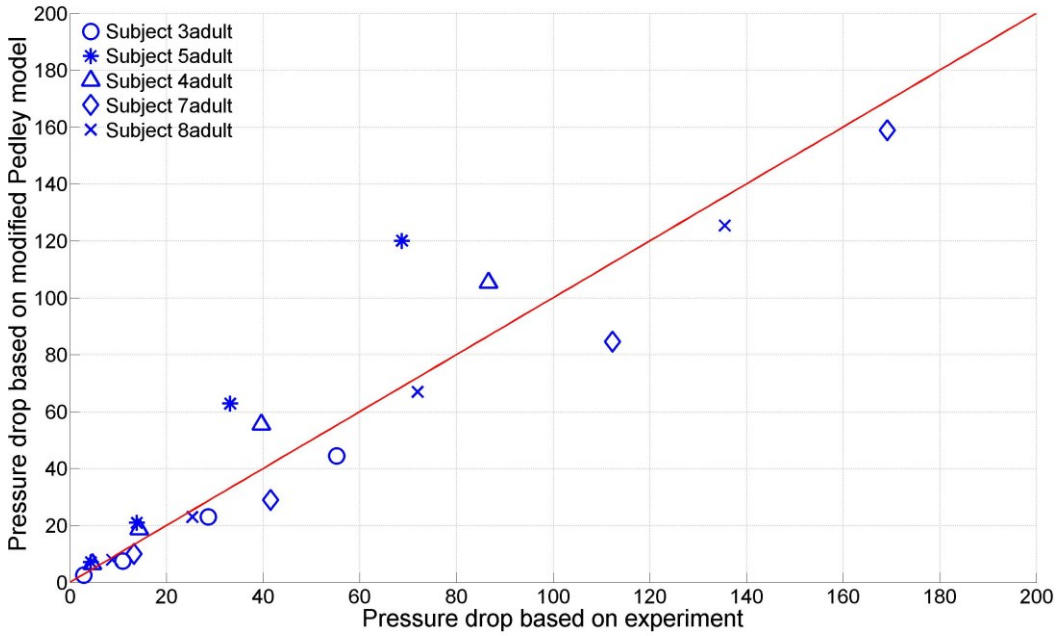

Figure 4.5: Comparison of pressure drop data predicted by the modified Pedley model (van Ertbruggen et al. 2005) with the measured data in adult replicas.

In calculating the pressure drop across the replicas, the distribution of flow through the branching airways is also calculated. Calculated values of the fraction of flow through the right lung are presented in Table 4.6. For both adults and child replicas, a greater fraction of the inhalation flow passes through airway of the right lung. The standard deviation between replicas was higher in the child group than in the adult group (0.15 versus 0.03 on average, respectively).

Table 4.6: Fraction of flow to the right lung. Data are presented as average (standard deviation). N=5 for the adult replicas, and =10 for the child replicas.

Flow rate (L/min)	Adult			Child		
	Katz model	Pedley model	Modified Pedley model	Katz model	Pedley model	Modified Pedley model
2	-	-	-	0.64(0.15)	0.63(0.15)	0.63(0.15)
5	-	-	-	0.64(0.15)	0.63(0.15)	0.63(0.15)
10	-	-	-	0.64(0.15)	0.63(0.15)	0.63(0.15)
15	0.58(0.02)	0.58(0.03)	0.58(0.04)	0.63(0.15)	0.63(0.15)	0.63(0.15)
30	0.58(0.02)	0.58(0.03)	0.58(0.04)	0.62(0.13)	0.63(0.15)	0.62(0.15)
60	0.57(0.02)	0.58(0.03)	0.58(0.04)	0.61(0.12)	0.62(0.15)	0.62(0.15)
90	0.56(0.02)	0.58(0.04)	0.58(0.04)	-	-	-

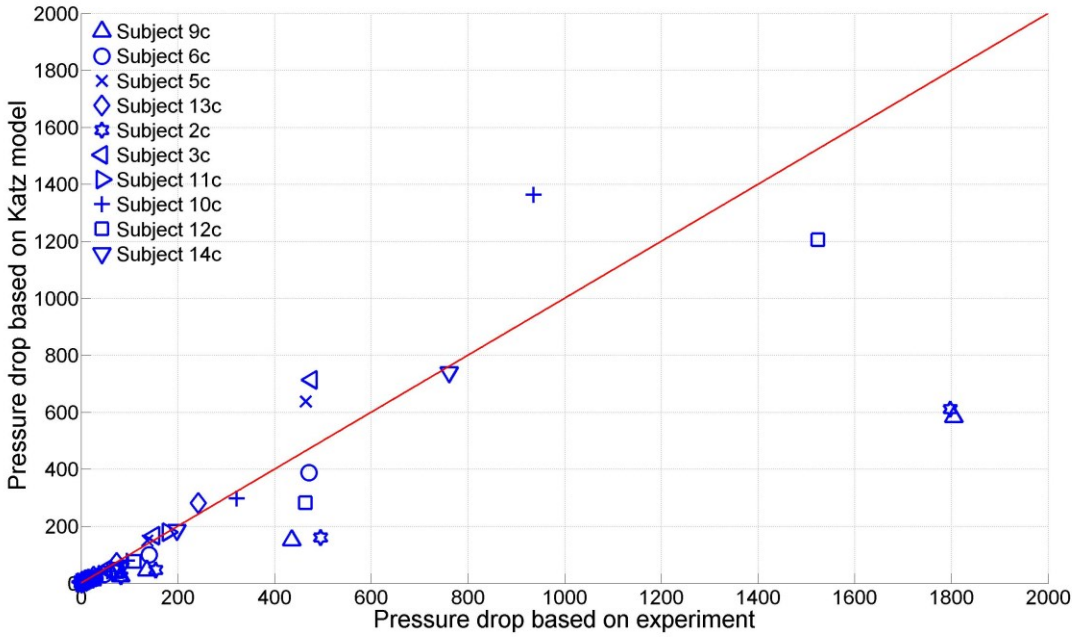

Figure 4.6a: Comparison of pressure drop data predicted by the Katz et al. (2010) model with the measured data in child replicas.

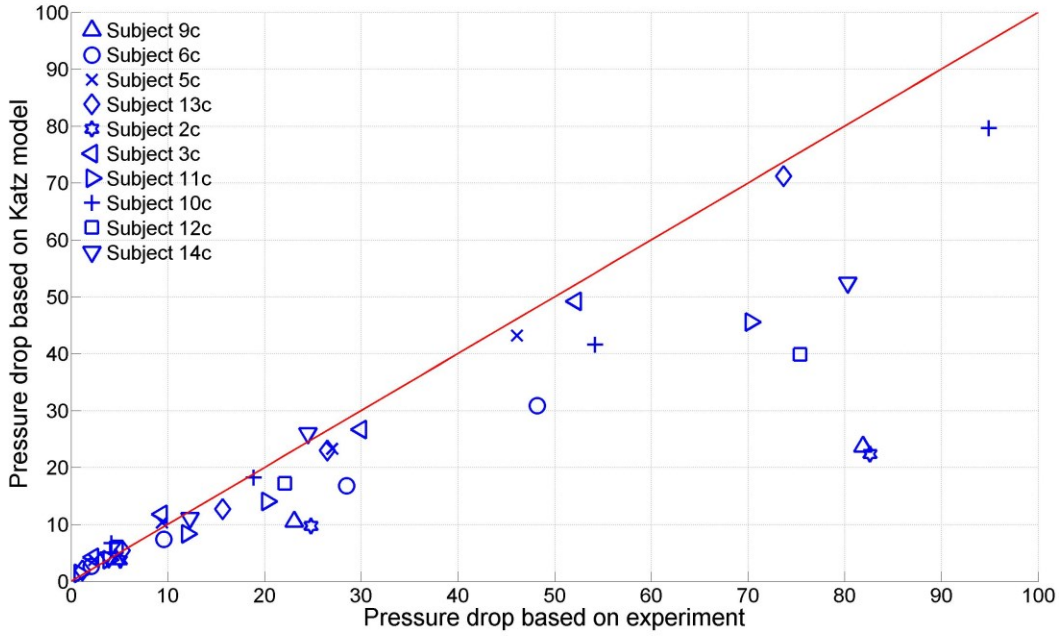

Figure 4.6b: Comparison of measured versus predicted pressure drop by the Katz et al. (2010) model in child replicas: magnified view in low range of pressure (0-100 Pa).

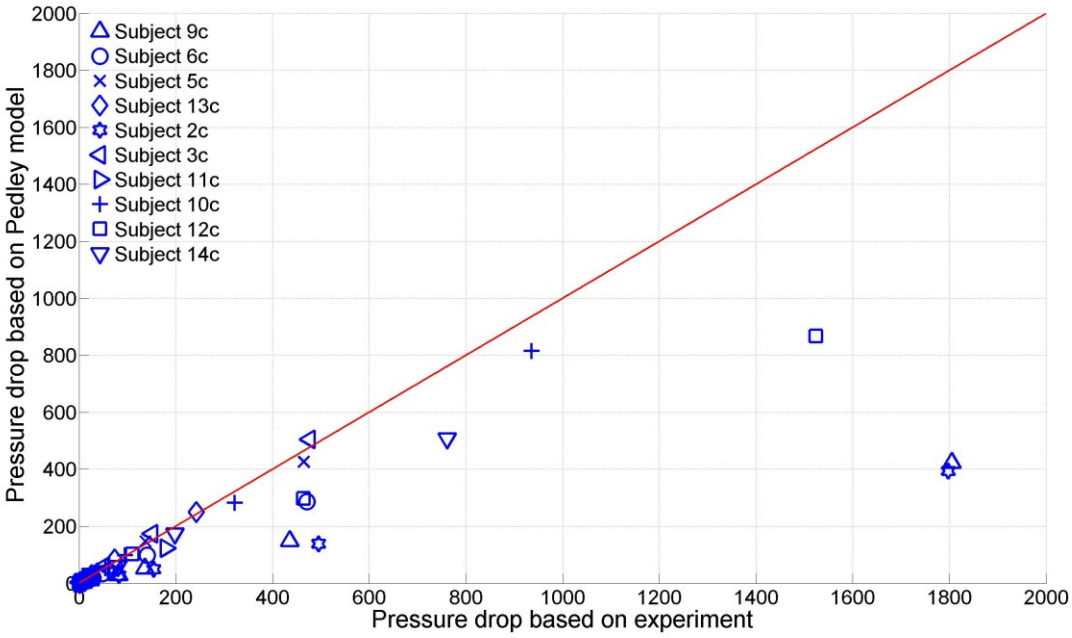

Figure 4.7a: Comparison of pressure drop data predicted by the Pedley et al. (1970) model with the measured data in child replicas.

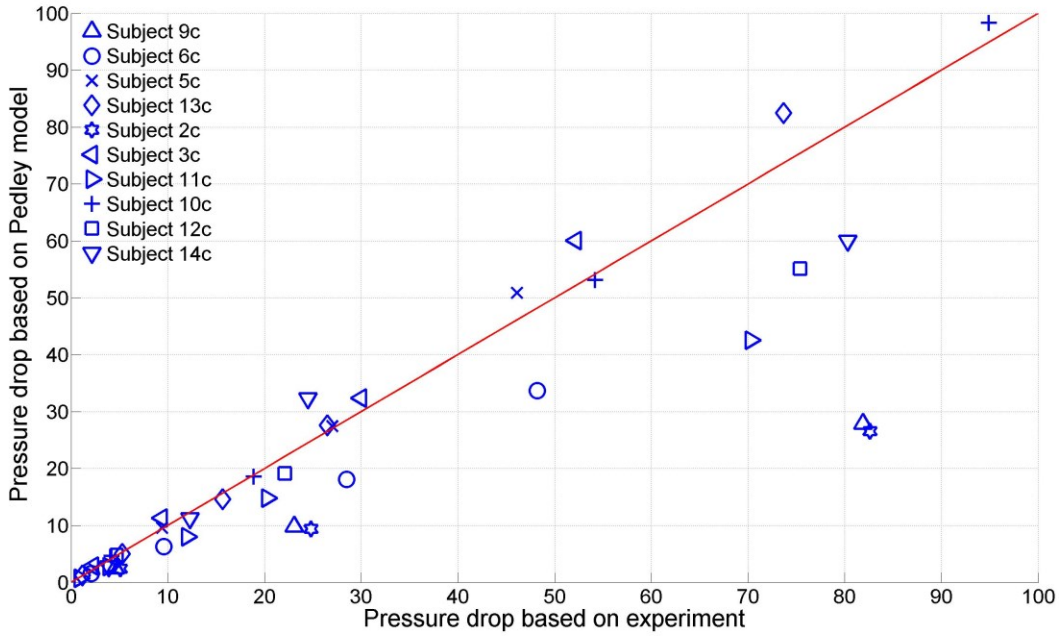

Figure 4.7b: Comparison of measured versus predicted pressure drop by the Pedley et al. (1970) model in child replicas: magnified view in low range of pressure (0-100 Pa).

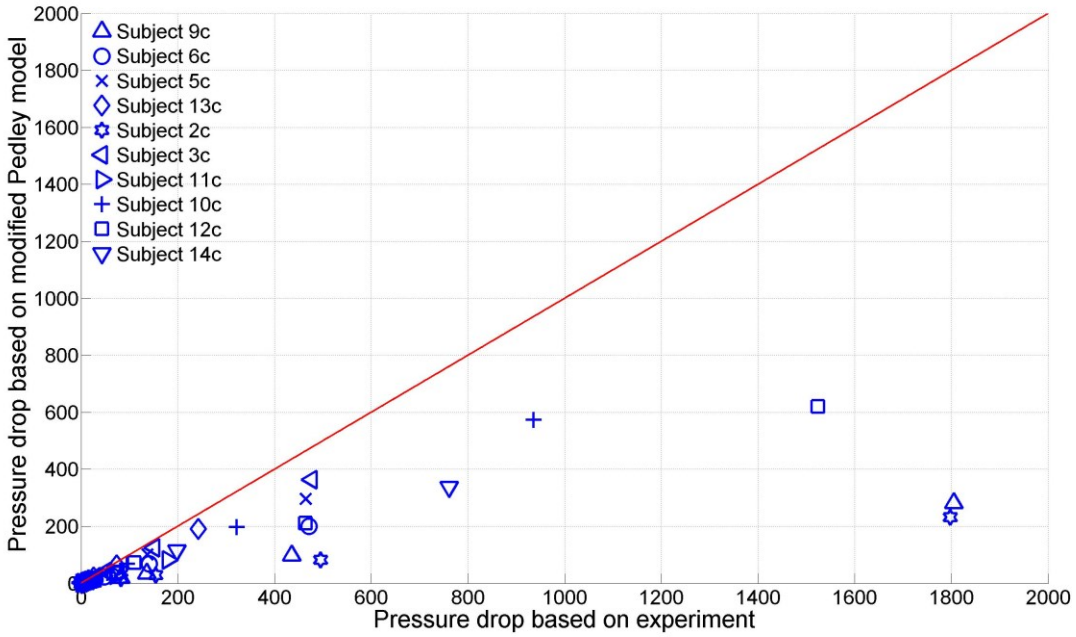

Figure 4.8a: Comparison of pressure drop data predicted by modified Pedley model (van Ertbruggen et al. 2005) with the measured data in child replicas.

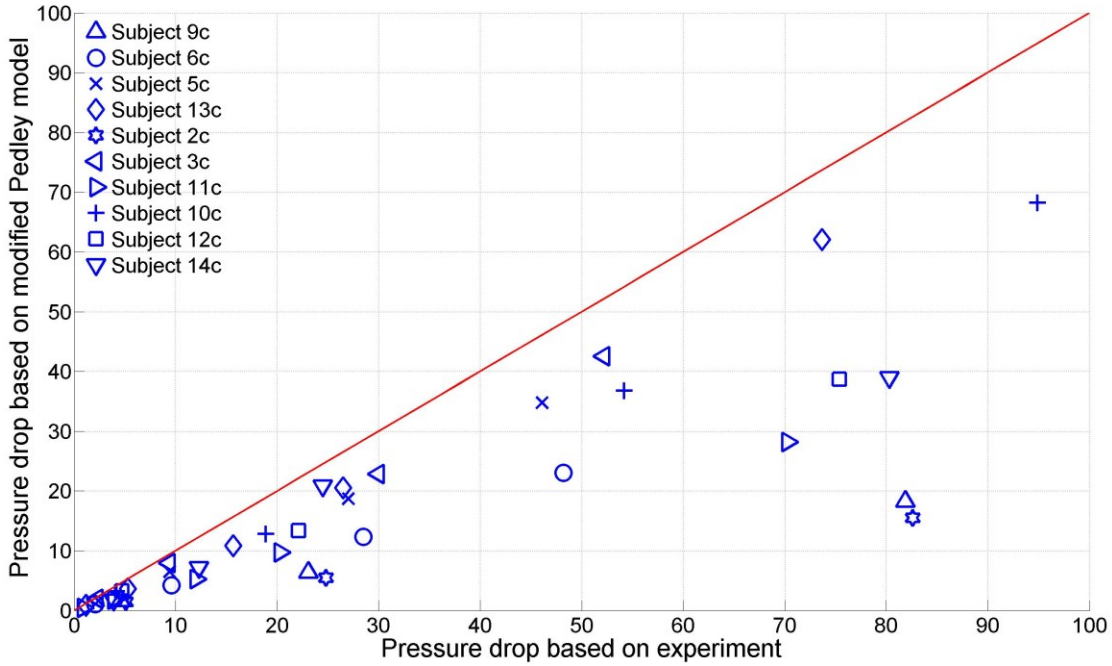

Figure 4.8b: Comparison of measured versus predicted pressure drop by the modified Pedley model (van Ertbruggen et al. 2005) in child replicas: magnified view in low range of pressure (0-100 Pa).

4.4 Discussion

In the present work, we measured pressure loss at varying flow rate through anatomically realistic conducting airway replicas of adults and children. Measured values were compared with values predicted using previous researchers' analytical airway resistance models developed based on measurements or simulations performed in adult conducting airway geometries. For the present five adult airways, the airway resistance model proposed by Pedley and colleagues (Pedley et al. (1970)) tended to over predict measured pressure loss. This is consistent with the results of previous CFD studies comparing predictions of conducting airway pressure loss made using the Pedley et al. model to simulated values (Comer et al. (2001); van Ertbruggen et al. (2005); Katz et al. (2011); Ismail et al. (2013)). Of the three resistance models evaluated, the modified Pedley model proposed by van Ertbruggen et al. (van Ertbruggen et al. (2005)) demonstrated closest agreement with our measured adult data. These authors modified the original Pedley model by proposing alternative coefficients for predicting the pressure loss through each proximal lung generation (as described above in Equation 4.11 and Table 4.3). The modified coefficients were based on pressure losses determined by CFD simulation of laminar flow through a single, representative, anatomically-based adult airway geometry. The good agreement of predicted pressure losses made using their model with our data in five different adult airway replicas, at tracheal Reynolds numbers exceeding 10,000 in the highest case (Table 4.5), was therefore not expected *a priori*. However, van Ertbruggen et al. (2005) argue that below Reynolds number averaging 8,000 the flow regime through conducting airways can be considered laminar or 'lightly' transitional, but not turbulent. Again with reference to Table 4.5, for a strong majority of cases we studied tracheal Reynolds numbers in the adult replicas that fell below 8,000. Furthermore, while variation in branching angle (and branching asymmetry) are not explicitly accounted for in the modified Pedley model, and surely existed between our five adult replicas, Kang et al. (2011) found only a weak influence of branching angle on simulated pressure loss through a model airway bifurcation. Based on comparison with our experimental results, we conclude that the modified Pedley model proposed by van Ertbruggen et al. (2005) accurately predicts central conducting airway resistance for adults across a wide range of inspiratory flow rates, from 15 to 90 L/min.

For the child airway replicas, predicted and measured pressure losses were generally in closer agreement for the Katz et al. (2010) model and the original Pedley et al. (1970) model than for the modified Pedley (van Ertbruggen et al. 2005) model.

Poorer agreement of the modified Pedley model with the child versus adult data may be due to differences in central conducting airway geometry between children and the single adult geometry used in creating this model, that are not captured explicitly in Equation 4.12 (recalling that model coefficients were fit to simulation data obtained in a representative single *adult* airway geometry).

All three models tended to under predict measured pressure loss at the highest flow rate studied in children (60 L/min), where tracheal Reynolds numbers averaged over 10,000. Indeed, for replicas from the youngest children studied (ages 4 and 5), the pressure loss at 60 L/min was sufficiently high that such an inspiratory flow rate is likely to be achieved *in vivo* by the corresponding child subjects only near maximum inspiratory effort (Vilozni et al.(2009)). At lower flow rates, corresponding to lower pressure loss, the original Pedley model (Pedley et al. (1970)) was the most accurate of the three models studied. Pedley et al. (1970) based their model on measurements made in idealized symmetric models of branching airways, where Reynolds number ranged from ~100 to ~1,000. Tracheal Reynolds numbers in our child replicas were on average within this range for the two lowest flow rates studied (2 and 5 L/min). This very likely explains the relatively close agreement between our measured data and predictions made using the Pedley model for low pressure loss (where flow rate and Reynolds number were also low) and lack of such agreement for higher pressure loss. For higher pressure loss, corresponding to higher flow rates and Reynolds numbers, none of the three models was consistently accurate for the child replicas; however, the Katz model (2011) performed somewhat better than the other models, possibly owing to its inclusion of turbulent losses at higher Reynolds numbers (Equations 4.13 and 4.14, above).

In calculating the total pressure loss through the airway replicas using each of the three airway resistance models, the distribution of flow through the replicas is also obtained. The fraction of flow directed to the right lung side of the replicas was found to average 0.58 in the adult replicas, with very little variation with flow rate or between replicas. This value is remarkably consistent with the distribution of ventilation to the right lung

observed *in vivo* (Lumb (2010)), especially given that for the intact, healthy, *in vivo* lung, ventilation distribution is determined more by downstream tissue compliance than by airway resistance (Swan et al. (2012)). Ostensibly, the dimensions of the central conducting airways act to reinforce, rather than oppose, this ventilation distribution. For the child replicas, the fraction of flow directed to the right lung side of the replicas (averaging 0.63) did not vary significantly from that for the adult replicas. However, variation between replicas was considerably greater for child than for adult replicas. This variation is potentially attributable to a greater variation in airway geometry for the child replicas, given that these geometries were obtained from images of children aged 4-8 years, and therefore at different stages of physical development.

4.5 Conclusion

Pressure loss was experimentally measured at varying flow rate through anatomically realistic conducting airway replicas of adults and children. Measured values were compared with values predicted using published analytical airway resistance models. The modified Pedley model proposed by van Ertbruggen et al. (2005) provided close agreement with measured central conducting airway resistance in adult replicas across a wide range of inspiratory flow rates, from 15 to 90 L/min. In contrast, in our child airway replicas, the Pedley et al. (1970) model predictions most closely match our experimental data, although all three resistance models underpredict pressure drops at the highest flow rates considered (60 L/min). Differences in the predictive accuracy of the resistance models at varying flow rates, and in adult versus child replicas, can be explained in part through consideration of the differing applicable Reynolds number ranges of the models.

4.6 References

Borojeni, A.A., Noga, M.L., Vehring, R., Finlay, W.H., 2014. Measurements of total aerosol deposition in intrathoracic conducting airway replicas of children. *Journal of Aerosol Science*. 73, 39-47.

Comer, J.K., Kleinstreuer C, Zhang Z., 2001. Flow structures and particle deposition patterns in double bifurcation airway models. 1. Airflow fields. Journal of Fluid Mechanics. 435, 25–54.

van Ertbruggen, C., Hirsch, C., Paiva, M., 2005. Anatomically based three-dimensional model of airways to simulate ow and particle transport using computational fluid ynamics. *Journal of Applied Physiology*. 98, 970-980.

Gemci, T., Ponyavin, V., Chen, Y., Chen, H., Collins, R., 2008. Computational model of airflow in upper 17 generations of human respiratory tract. *Journal of Biomechanics*. 41(9), 2047-2054.

Horsfield, K., Dart, G., Olson, D.E., Filley, G.F., Cumming, G., 1971. Models of the human bronchial tree. *Journal of Applied Physiology*. 31, 207–217.

Ismail, M., Comerford, A., Wall, W.A., 2013. Coupled and reduced dimensional modeling of respiratory mechanics during spontaneous breathing. *International Journal For Numerical Methods In Biomedical Engineering*. 29, 1285-1305.

Kang, M-Y, Hwang, J., and Lee, J-W., 2011. Effect of geometric variations on pressure loss for a model bifurcation of the human lung airways. *Journal of Biomechanics*. 44, 1196–1199.

Katz, I.M., Martin, A.R., Muller, P.-A., Terzibachi, K., Feng, C.-H., Caillibotte, G., Sandeau, J., Texereau, J., 2011. The ventilation distribution of helium-oxygen mixtures and the role of inertial losses in the presence of heterogeneous airway obstructions. *Journal of Biomechanics*. 44, 1137-1143.

Lumb, A.B., 2010. *Nunn's Applied Respiratory Physiology*, Seventh Edition. Elsevier Ltd.

Otis A.B., Bembower W.C., 1949. Effect of gas density on resistance to respiratory gas flow in man. *Journal of Applied Physiology*. 2, 300-306.

Otis A.B., Fenn W.O., Rahn H., 1950. Mechanics of Breathing in Man. *Journal of Applied Physiology*. 2, 592-607.

Otis A.B., McKerrow C.B., Bartlett R.A., Mead J., McIlroy M.B., Selverstone N.J., Radford E.P., 1956. Mechanical factors in distribution of pulmonary ventilation. *Journal of Applied Physiology*. 8, 427-443.

Pedley, T.J., Schroter, R.C., Sudlow, M.F., 1970. Energy losses and pressure drop in models of human airways. *Journal of Respiration Physiology*. 9, 371-386.

Rohrer, F., 1915. Der Strömungswiderstand in den menschlichen Atemwegen und der Einfluss der unregelmässigen Verzweigungen des Bronchialsystems auf den Atmungsverlauf in verschiedenen Lungenbezirken. *Pflügers Arch ges Physiol*, 162, 225–299.

Swan, A.J., Clark, A.R., Tawhai, M.H., 2012. A computational model of the topographic distribution of ventilation in healthy human lungs. *Journal of Theoretical Biology*. 300, 222-231.

Vilozni, D., Efrati, O., Barak, A., Yahav, Y., Augarten, A., Bentur, L., 2009. Forced inspiratory flow volume curve in healthy young children. Pediatric Pulmonology. 44(2), 105-111.

White, F. M., 2010. *Fluid Mechanics, 7th edition*. Boston, USA: McGraw-Hill.

Wilquem, F., Degrez. G., 1997. Numerical modeling of steady inspiratory airflow through a three-generation model of the human central airways. *Journal of Biomechanical Engineering*. 119(1), 59-65.

CHAPTER 5: CAN DOWNSCALING THE ALBERTA IDEALIZED CHILD THROAT PREDICT DOSE-TO-LUNG DEPOSITION FROM PRESSURIZED METERED DOSE INHALERS IN 5-7 YR OLD CHILDREN?

5.1 Introduction

5.1.1 Background

Aerosols in the form of commercial pressurized metered dose inhaler (pMDI) such as QVAR® are commonly used for therapeutic treatment of lung diseases. Asthma is the most common pulmonary disease in children (Ahrens (2005)). MDIs are considered as effective devices in the clinical treatment of acute asthma in infants and children (Amirav and Newhouse (1997)). The amount of deposited pharmaceutical particles in the conducting and distal airways (the lung dose) following inhalation is an important parameter in clinical respiratory drug delivery and in evaluating the efficiency of drug delivery devices. Quantifying the amount deposited in lung airways is difficult (Newman et al. (2008)) and researchers are interested in finding *in vitro* correlations to predict *in vivo* deposition data in this part of human lung (Newman et al. (2008), Schroeter et al. (2014)). From a drug delivery point of view, the total lung dose can be quantified by the dose delivered to the distal airways of the extrathoracic region (Finlay and Martin (2008)). Thus, measuring aerosol deposition in intrathoracic conducting airways is of interest in evaluating the efficiency of the inhalation drug delivery devices. For this purpose, the idealized replica of pediatric conducting airways that has already been presented in an earlier chapter is of interest. However, to use this replica with a metered dose inhaler requires an extrathoracic airway replica that allows connection to the mouthpiece of the pMDI. In this chapter, the previously developed Alberta Idealized Child Throat (Golshahi and Finlay (2012)) can be considered. This geometry mimics average deposition in 6-14 year old children, which is older than the age range considered in developing our idealized conducting airway geometry (4-8 year olds). To overcome this mismatch, one possibility is to downscale the Alberta Idealized Child Throat so that its trachea matches the tracheal diameter of our 4-8 year old idealized conducting airway geometry. However, the ability of the Alberta Idealized Child Throat to mimic throat deposition in the younger age group (4-8 year olds) used to develop our intrathoracic conducting airway geometry is not known. In this chapter, we explore this issue.

5.1.2 Pharmaceutical aerosols in the form of metered dose inhalers (pMDIs)

Employing drug delivery devices such as pMDIs for inhalation therapy of respiratory tract disease offers advantages compared to other routes of drug administration (Finlay (2001)). QVAR® (QVAR®, Medicis Pharmaceutical Corporation, Scottsdale, AZ, USA) is the pressurized metered dose inhaler (pMDI) that delivers beclomethasone dipropionate (BDP) as the main medicinal ingredient, a corticosteroid medicine that used to lessen the severity of asthma attacks. The dosage of the QVAR® (label claim) is 100 micrograms of BDP per each puff.

5.2 Methodology

5.2.1 Fabrication of Child Idealized Throat

The Alberta Idealized Child Throat model proposed as the isotropically scaled down version of the Alberta Idealized Throat mimics gives average extrathoracic deposition in children aged 6 to 14 years old (Golshahi and Finlay (2012)). The Idealized Child Throat has been successfully used to compare the *in vitro* deposition of pharmaceutical aerosols with *in vivo* deposition in the extrathoracic airway of children in this age range (Ruzycki et al. (2014)).

5.2.2 Mouth Throat Model

The Idealized Child Throat was scaled down to provide a suitable inlet geometry for the idealized central conducting airways. The Idealized Child Throat was downscaled by a uniform factor of 0.9, to match its tracheal diameter with that of the idealized conduting airways described in an earlier chapter. Thus, its trachea was scaled to have a diameter of 8.96 mm. This downscaled throat was built using ABS (Acrylonitrile butadiene styrene) plastic. Fabrication of the plastic idealized mouth-throat model was done using a Stereo-Lithography rapid prototyping technique (Objet Eden350V 3D printer, Stratasys, Inc., Eden Prairie, MN).

5.2.3 Experimental set-up

A schematic diagram of the experimental setup is shown in Fig. 5.1. The pMDI device, scaled version of the Idealized Child Throat, and downstream collection filter are connected to a vacuum pump through flexible teflon tubing. A constant flow rate (33 L/min) was set by a

control valve and monitored by a digital mass flowmeter (4000 series, TSI Inc., USA) during each trial.

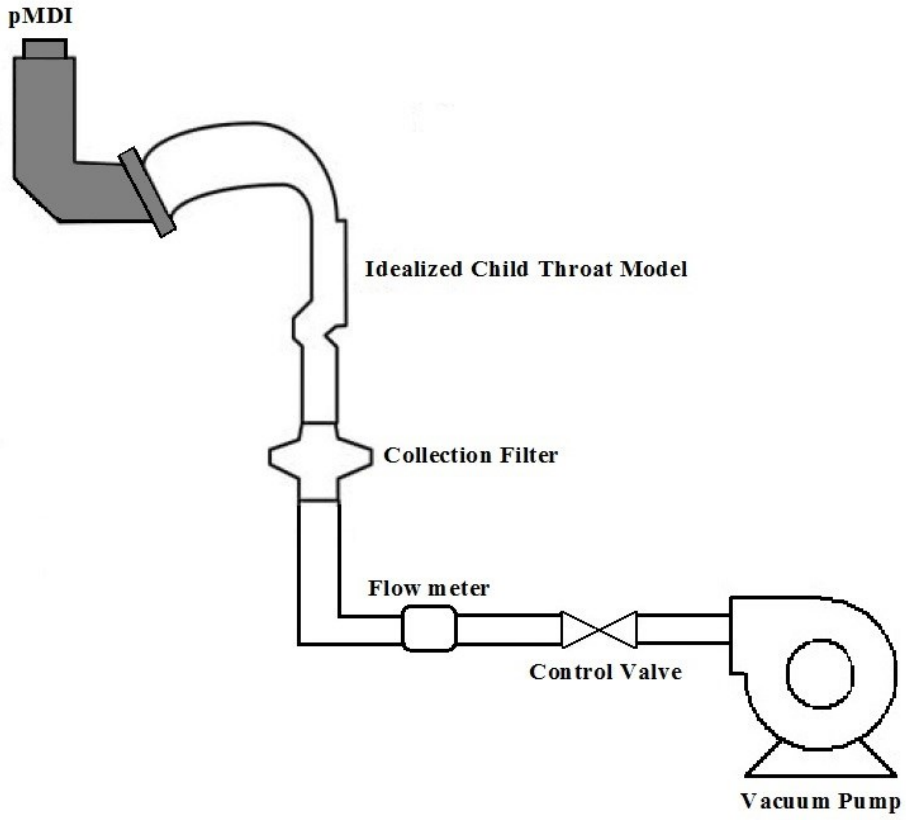

Figure 5.1: Experimental set-up for *in vitro* pMDI test

5.2.4 *In vitro deposition measurement*

Prior to the experiment, the pMDI container was primed by actuating into the air twice. In order to measure the amount of delivered dose i.e. the amount of drug dose leaving the device and reaching the patient per each actuation, the inhaler device was connected directly to a filter (Respir Gard II^{TM}, Vital Signs Inc., a GE Health care Co., Englewood, CO, USA) and downstream vacuum pump. The mass of beclomethasone dipropionate deposited on this filter was determined by chemical assay using ultraviolet (UV) spectroscopy (model 8452A, Hewlett Packard, Greely, Ontario, Canada). The same assay was used to determine mass of drug delivered to the filter with the idealized model in place as in Figure 5.1.

The constant inhalation flow rate was determined based on the average inhalation flow rate of 10 child subjects aged 4-8 years old investigated in our previous study (Borojeni et al. (2014)). The height of each subject was reported elsewhere (Borojeni et al. (2014)). Stocks and Quanjer correlations (Stocks et al. (1995)) were used to calculate the inspiratory capacity of each subject. The resulting average inspiratory capacity of all 10 child subjects was 1 L.

Mean inspiration time can be calculated as the time difference between total inspiratory time and time of actuation. The total inspiratory time for the subjects aged 4-8 years old was considered 2.16 sec., according to the age group 5-7 years old reported by Devadason et al. (2003). The time of inhaler actuation for this age group was considered as 0.29 sec. (Devadason et al. (2003)). Thus, the mean inspiratory time for this age group is 1.87 sec. This results in an average inhalation flow rate, for our 10 subjects, of 33 L/min, which is not dissimilar from the value of 28 L/min given by Devadason et al. (2003) for their 5-7 year olds. This choice of calculated flow rate also seems reasonable as it is close to the reported *in vivo* data from the literature (Pedersen and Mortensen (1990)). Pedersen and Mortensen (Pedersen and Mortensen (1990)) reported all children aged 3-10 years old in their study while inhalation via the metered dose inhaler generated inhalation flow rate of 35 (L/min).

The experiment was repeated five times and the lung deposition defined as the dose depositing on the collected filter downstream of the Mouth Throat model.

5.3 Results

5.3.1 In vitro experiments

The *in vitro* deposition on the collective filter was compared with *in vivo* data from the literature. Mean deposition of the QVAR pMDI measured in the downstream filter coupled directly to the Mouth Throat model is shown in Figure 5.2. It was observed that the measured lung deposition from the collection filter is higher than the *in vivo* value measured previously by Devadason et al. (Devadason et al. (2003)) for children aged 5-7 years old. Devadason et al. (Devadason et al. (2003)) reported mean lung deposition as 36.9% of delivered dose. However, our measured *in vitro* lung deposition is 60% of delivered dose. The much higher deposition in the downstream filter is because of too little deposition in the scaled throat. This implies that downscaling the Alberta Idealized Child Throat does not appear to provide an accurate throat model for attaching upstream of our previously described idealized child conducting airways. In chapter 3 it was

shown that our idealized pediatric central conducting airway model could mimic average total particle deposition in children aged 4-8 years old reasonably well. The Alberta Idealized Child Throat has previously been shown to predict average extrathoracic deposition in children aged 6 to 14 years (Ruzycki et al. (2014) and Golshahi and Finlay (2012)). Despite these successes, the present data indicates that scaling down the Child Idealized throat to fit the idealized pediatric central conducting airway model is not expected to allow mimicking of lung deposition in children aged 4-8 years old.

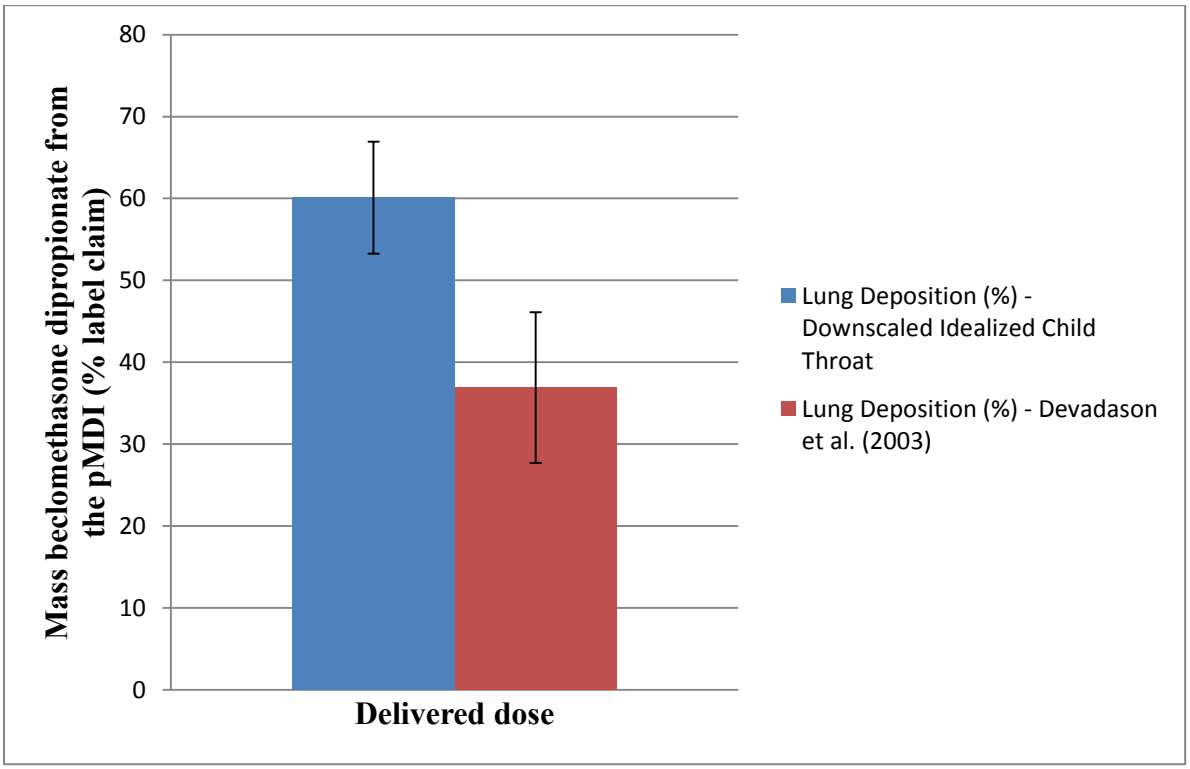

Figure 5.2: Mean deposition of the QVAR pMDI measured in the downstream filter coupled directly to the downscaled Mouth Throat model. Error bar indicates the standard deviation of the 5 replicates of the experiment.

5.4 Discussion

5.4.1 Comparison of in vitro data with the in vivo data

Comparison of deposition in the downstream filter vs. lung deposition measured during oral inhalation *in vivo* previously by Devadason et al. (Devadason et al. (2003)) for children aged 5-7 years old using pMDI is depicted in Fig. 5.2. The higher deposition in the downstream filter,

assumed here to equal lung deposition, suggests that downscaling the Idealized Child Throat might not provide a suitable mouth-throat geometry for this age group (4-8 years old). Previous researchers have noted the different pattern of aerosol deposition between adult and child mouth-throat models (Bickmann et al. (2008)). Others have noted that the mouth-throat geometry of young children may not simply be a miniature scale of the adult mouth-throat geometry (Ahrens (2005)). This may partly explain the inability of the present downscaled idealized child throat to match the in vivo data.

An additional factor that may confound the present comparison is the use of plastic material for the downscaled throat, which does not allow accurate mimicking of electrostatic effects on deposition (Azhdarzadeh et al. (2014)). In addition, ambient humidity can affect throat deposition (Shemirani et al. (2013)), and the humidity of the *in vivo* experiments of Devadason et al. 2003 that we are comparing to is not known. Despite these issues, the present lack of agreement between our downscaled throat and the *in vivo* data of Devadason et al. (2003) suggests that further work is needed if a suitable mouth-throat mimic is to be developed as an entry port for our 4-8 year old conducting airway.

5.5 Conclusions

The measured deposition data in the downstream filter indicates that scaling down the Child Idealized throat to fit the idealized pediatric central conducting airway model does not mimic lung deposition in children aged 4-8 years old accurately for the present pMDI (QVAR®) device when compared to published *in vivo* data.

5.6 References

Amirav I. and M. T. Newhouse. Metered-Dose Inhaler Accessory Devices in Acute Asthma. Efficacy and comparison with nebulizers: a literature review. *Arch Pediatr Adolesc Med*. 1997;151:876-882.

Ahrens R.C. The role of the MDI and DPI in pediatric patients: “children are not just miniature adults”. *Respir Care*. 2005;50(10):1323-8.

Azhdarzadeh, M., Olfert, J. S., Vehring, R., W. H. Finlay. Effect of induced charge on deposition of uniformly charged particles in a pediatric oral-extrathoracic airway. *Aerosol Science and Technology.* 2014:48:508-514.

Bickmann D., Wachtel, H., Kroger, R., Langguth, P. Examining inhaler performance using a child’s throat model. *Respiratory Drug Delivery*. 2008:2:565-570.

Devadason S. G., Huang T., Walker S., Troedson R., Le Souef P. N. Distribution of technetium-99m-labelled QVAR ™ delivered using an Autohaler ™ device in children. *European Respiratory Journal*. 2003:21:1007-1011.

Warren H. Finlay. The mechanics of inhaled pharmaceutical aerosols: an introduction. *Academic Press*, 2001.

Finlay W.H. and Martin A.R. Recent advances in predictive understanding of respiratory tract deposition. *Journal of Aerosol Medicine and Pulmonary Drug Delivery*. 2008:21(2):189-205.

Golshahi L. and W. H. Finlay. An idealized child throat that mimics average pediatric oropharyngeal deposition. *Journal of Aerosol Science and Technology*. 2012:46:i-iv.

Newman S. P., Chan H-K. *In vitro*/*in vivo* comparisons in pulmonary drug delivery. *Journal of Aerosol Medicine and Pulmonary Drug Delivery*. 2008:21(1):77-84.

Pedersen S. and S. Mortensen. Use of different Inhalation Devices in Children. *Lung*. 1990:Suppl:653-657.

Ruzycki CA, Golshahi L., Vehring R, Finlay WH. Comparison of *In vitro* deposition of Pharmaceutical aerosols in an Idealized Child Throat with *In vivo* Deposition in the Upper Respiratory Tract of Children. *Pharm Res J*. 2014:

Schroeter JD, Holt JT., Asgharian B., Bovet JM., Hickey AJ. Characterization of particle size distributions and respiratory tract deposition of Albuterol Sulfate Metered Dose Inhalers. RDD 2014:345-348.

Shemirani, F. M., Hoe, S., Lewis, D., Church, T., Vehring, R., W. H. Finlay. *In vitro* investigation of the effect of ambient humidity on regional delivered dose with solution and suspension MDIs. *J of Aerosol Med Pulm Drug Delivery*. 2013:26(4):215-222.

Stocks J, Quanjer PH. Reference values for residual volume, functional residual capacity and total lung capacity: ATS workshop on lung volume measurements official statement of the European respiratory society. *Eur Respir J*. 1995;8(3):492-506.

Wachtel H., Bickmann, D., Breitkreutz, J., Langguth, P. Can pediatric throat models and air flow profiles improve our dose finding strategy? *Respiratory Drug Delivery*. 2010;1:195-204.

Zhang Y, Gilbertson K., Finlay WH. *In vivo-In vitro* Comparison of Deposition in Three Mouth-Throat Models with Qvar® and Turbuhaler® Inhalers. Journal of Aerosol Medicine. 2007:20(3):227-235.

CHAPTER 6: CONCLUSIONS AND FUTURE WORK

6.1 Summary and Conclusions

In this thesis, a correlation that quantitatively predicts micrometer-sized aerosol particle deposition in the central conducting airways (trachea to generation 3) of children and adults was validated with the experimental data. Experiments were conducted using steady inhalation airflow rates to measure the deposition of monodisperse particles with diameters of 3.5–5.5 μm in replicas of the upper tracheobronchial airways of 11 children aged 2–8 years. The total deposition of particles was measured in each replica using gravimetry. Validation was performed by measuring deposition in five adult replicas and comparing with existing published data. Although there is considerable intersubject variability in our data, the empirical correlation of Chan &Lippmann (1980) was found to predict total deposition reasonably well in all of our adult and child replicas.

Moreover, the development of an idealized pediatric central conducting airway model representing 4-8 years old children for the purpose of mimicking average total particle deposition was obtained in this thesis. Dimensions of the idealized model were selected based on analytical prediction of deposition in scaled versions of existing adult airway geometries. Validation experiments were conducted using steady inhalation air flow rate to measure the deposition of monodisperse particles with mass median diameters (MMD) of 3.5, 4.5, 5 and 5.2 μm in the idealized pediatric model. The total deposition of particles was measured using gravimetry. Experimental data confirmed that aerosol deposition in the idealized pediatric central conducting airway geometry was consistent with the average deposition previously measured in 10 realistic airway replicas for children 4-8 years old. For development of inhaled pharmaceutical products, an idealized geometry that mimics average deposition in the pediatric population is desirable.

Furthermore, the accuracy of airway resistance models was validated with experimental data in predicting pressure drop across anatomically realistic conducting airway replicas for adults and children. Predicted data from various previously-published airway resistance models was in reasonable agreement with measured pressure drop in both adult and child replicas.

Finally, the Child Idealized throat developed in this research group (Golshahi and Finlay (2012)) was downscaled to fit the idealized pediatric central conducting airways. The ability of the downscaled Child Idealized throat to mimic pediatric lung dose measured *in* vivo for a commercial pMDI by Devadason et al. (Devadason et al. (2003)), was evaluated as a part of this thesis. The present data indicates that scaling down the Child Idealized throat to fit the idealized pediatric central conducting airway model did not provide good estimation of the *in vivo* data in children aged 4-8 years old.

6.2 Future Work

In this thesis, the focus has been on *in vitro* measurement of the total deposition in central conducting airways (trachea to generation 3) of adults and children during inhalation only, since the lower tracheobronchial and alveolar regions of human lung would be needed to simulate the exhaled breath condition accurately. It has recently been shown that the accurate geometry of the airways has a significant effect on the fate of inhaled aerosols (Nowak et al. (2003); Annapragada and Mishchiy (2007)). Therefore, studies are needed to simulate tracheobronchial and alveolar geometries to measure the intrathoracic aerosol deposition during exhalation.

Lastly, the analytical engineering models were applied to the anatomical-accurate airway replicas to predict airway pressure drop during inhalation. The predicted data was comparable to the experimental *in vitro* data in the realistic casts. The predicted pressure drop through right and left lung airways of each replica was analytically calculated in this study. *In vitro* experiments are also recommended to measure pressure drop of each lung airway split. Validation of the developed airway resistance models to predict pressure drop in the right and left lung airways with the measured *in vitro* experimental data can be a topic of future research.

6.3 References

Annapragada, A. and N. Mishchiy. *In silico* modeling of aerosol deposition in lungs. *Drug Discovery Today: Disease Models.* 4(3):155-161, 2007.

Devadason S. G., Huang T., Walker S., Troedson R., Le Souef P. N. Distribution of technetium-99m-labelled QVAR ™ delivered using an Autohaler ™ device in children. *European Respiratory Journal*. 2003:21:1007-1011.

Golshahi L. and W. H. Finlay. An idealized child throat that mimics average pediatric oropharyngeal deposition. *Journal of Aerosol Science and Technology*. 2012:46:i-iv.

Nowak, N., Kalkade, P. P., Annapragada, A. V. Computational fluid dynamics simulation of airflow and aerosol deposition in human lungs. *Annals of Biomedical Engineering*. 31(4): 374-390, 2003.